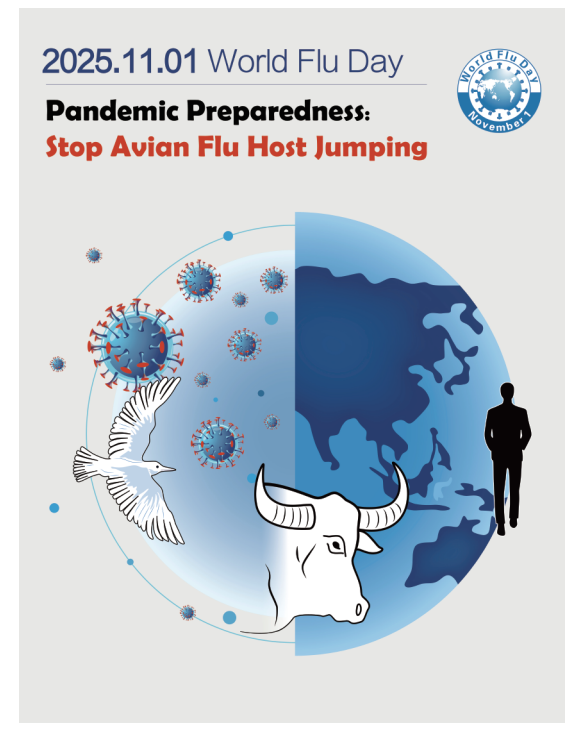
CHINA CDC WEEKLY

Vol. 7 No. 44 Oct. 31, 2025 Weekly

中国疾病预防控制中心周报



WORLD FLU DAY ISSUE

Commentary

Preparing for the Next Influenza Pandemic: Vaccine Progress, Challenges, and Prospects

1377

Vital Surveillances

Epidemiological Assessment and Optimization of School-Based Influenza Vaccination — Shenzhen City, Guangdong Province, China, 2023–2024

1383

Phylogenetic and Molecular Characteristics of An H3N8 Avian Influenza Virus Detected in Wild Birds — Beijing, China, September 2024

1389

Methods and Applications

Developing Machine Learning Prediction Model for Daily Influenza Reported Cases Using Multichannel Surveillance Data — A City, Hubei Province, China, 2023–2025

1396

Outbreak Reports

Epidemiological and Genetic Characterization of Three H9N2 Viruses Causing Human Infections — Changsha City, Hunan Province, China, April 2025

1403







China CDC Weekly

Editorial Board

Editor-in-Chief Hongbing Shen **Founding Editor** George F. Gao

Deputy Editor-in-Chief Liming Li Gabriel M Leung Zijian Feng

Executive Editor Chihong Zhao **Members of the Editorial Board**

Rui Chen Wen Chen Xi Chen (USA) Zhuo Chen (USA) Ganggiang Ding Xiaoping Dong Pei Gao Mengjie Han Yuantao Hao Na He Yuping He Guoqing Hu Zhibin Hu Yuegin Huang Na Jia Weihua Jia Zhongwei Jia Guangfu Jin Xi Jin Biao Kan Ni Li Haidong Kan Qun Li Ying Li Zhenjun Li Min Liu Qiyong Liu Xiangfeng Lu Jun Lyu Huilai Ma Jiaqi Ma Chen Mao Xiaoping Miao Ron Moolenaar (USA) Daxin Ni An Pan William W. Schluter (USA) Lance Rodewald (USA) Yiming Shao Xiaoming Shi Yuelong Shu RJ Simonds (USA) Xuemei Su Chengye Sun Quanfu Sun Feng Tan Xin Sun **Jinling Tang Huaging Wang** Hui Wang Linhong Wang Tong Wang Guizhen Wu Jing Wu Xifeng Wu (USA) Yongning Wu Min Xia Ningshao Xia Yankai Xia Lin Xiao Zundong Yin Dianke Yu Hongjie Yu Hongyan Yao Shicheng Yu Ben Zhang Jun Zhang Liubo Zhang Wenhua Zhao Yanlin Zhao Xiaoying Zheng Maigeng Zhou

Advisory Board

Xiaonong Zhou

Director of the Advisory Board Jiang Lu

Vice-Director of the Advisory Board Yu Wang Jianjun Liu Jun Yan **Members of the Advisory Board**

Guihua Zhuang

Chen Fu Gauden Galea (Malta) Dongfeng Gu Qing Gu Yan Guo Ailan Li Jiafa Liu Peilong Liu Yuanli Liu Kai Lu Roberta Ness (USA) **Guang Ning** Minghui Ren Chen Wang Hua Wang Kean Wang Xiaoqi Wang Zijun Wang Fan Wu Xianping Wu Jingjing Xi Jianguo Xu Gonghuan Yang Tilahun Yilma (USA)

Guang Zeng Xiaopeng Zeng Yonghui Zhang Bin Zou

Editorial Office

Directing Editor Chihong Zhao
Managing Editors Yu Chen
Senior Scientific Editors

Xuejun Ma Daxin Ni Ning Wang Wenwu Yin Shicheng Yu Jianzhong Zhang Qian Zhu

Scientific Editors

Weihong Chen Tao Jiang Xudong Li Nankun Liu Liwei Shi Liuying Tang Meng Wang Zhihui Wang Qi Yang Qing Yue Lijie Zhang Ying Zhang

Cover Image: adapted from Drs Ke Lan and William Jun Liu.

Commentary

Preparing for the Next Influenza Pandemic: Vaccine Progress, Challenges, and Prospects

Na Zhang¹; Dayan Wang¹,#

ABSTRACT

Influenza pandemics arise when novel influenza virus subtypes emerge in populations with little or no pre-existing immunity. The recent expansion of H5N1 _ circulation in mammals including documented spread in cattle and sporadic human infections — coupled with the emergence of mutations pandemic potential, associated with enhanced underscores the persistent threat of novel influenza strains. Pandemic preparedness critically depends on developing effective vaccines capable of providing broad protection across diverse viral strains. While vaccination remains the most effective strategy for preventing influenza and its complications, pandemic vaccine development faces substantial challenges. These include the rapid mutation rates characteristic of influenza viruses, driven by error-prone RNA replication, broad host range, environmental selection pressures, and frequent genetic recombination. Such factors complicate predictions of which strain will trigger the next pandemic and hinder efforts to create universal vaccines. Recent advances in vaccine production platforms, bioinformatics, and artificial intelligence have accelerated pandemic vaccine development capabilities. Continued research is essential to enhance vaccine technology, expedite production timelines, and broaden vaccine efficacy against the full spectrum of influenza virus strains.

Influenza is an acute respiratory disease caused by influenza viruses, characterized by rapid viral mutations that occur through antigenic drift and antigenic shift. This disease has posed a persistent threat to global public health, with seasonal epidemics occurring annually and occasional pandemics that can have farreaching consequences (*1*–*2*). An influenza pandemic is defined by the global spread of a novel influenza A virus subtype, against which most of the world's population possesses little or no pre-existing immunity,

resulting in rapid international transmission. The 1918 Influenza Pandemic, caused by the H1N1 influenza virus, resulted in an estimated 50 million deaths worldwide (with some estimates reaching 100 million) and significantly reduced global life expectancy by 10–12 years, marking it as one of the most catastrophic public health events in human history. Subsequent pandemics — including the 1957 H2N2 influenza, the 1968 H3N2 influenza, and the 2009 H1N1 influenza — were generally less severe than the 1918 event but nonetheless remained serious threats to human life and economic stability (3). The substantial impacts of influenza pandemics on global public health, economies, and societies underscore the critical importance of effective preparedness and response strategies to reduce pandemic severity, save lives, and minimize socio-economic disruptions. represent the most effective intervention for preventing influenza and its complications. However, developing vaccines for pandemic influenza viruses presents significant challenges. The virus mutates rapidly, and predicting which strain will trigger the next pandemic remains difficult. Here we address the progress, challenges, and prospects for vaccine development in preparation for the next influenza pandemic.

Etiological Basis of Influenza Pandemics

Pandemic influenza strains primarily arise from reassortment between human seasonal influenza viruses and zoonotic influenza viruses. For example, the hemagglutinin (HA), neuraminidase (NA), and polymerase basic protein 1 (PB1) genes of the 1957 H2N2 influenza pandemic strain originated from avian influenza viruses; the NA and PB1 genes of the 1968 H3N2 influenza strain were similarly avianderived; and the 2009 H1N1 influenza strain emerged from a triple reassortment involving human, avian, and swine influenza viruses (4).Consequently, strengthening surveillance and research on animal influenza viruses, particularly avian influenza viruses, is essential for pandemic preparedness. The potential threats posed by H7N9 and H5Nx subtypes warrant particular attention (5). Historically, H7N9 viruses

acquired dual receptor-binding capability (recognizing both avian α 2,3-linked and human α 2,6-linked sialic acid receptors) through G186V and Q226L mutations in their HA protein, thereby identifying these viruses as high-pandemic-risk candidates (6). Similarly, H5Nx viruses have demonstrated extensive global spread and host adaptability since their first emergence in humans in 1997. Among these subtypes, H5N1 and H5N6 pose the greatest threat to humans, with case fatality rates exceeding 50% (7-8). Since 2021, H5Nx clade 2.3.4.4b viruses have caused large-scale outbreaks in avian populations, subsequently expanding to infect over 48 genera of terrestrial and marine mammals, including cattle, thereby elevating the risk of novel virus emergence (9-10). Notably, dual receptor (α 2,3 and α 2,6) binding capacity has been documented for bovine clade 2.3.4.4b H5N1 highly pathogenic avian influenza viruses (HPAIVs), which, combined with mammalian-adaptive mutations such as E627K in the polymerase basic protein 2 (PB2) protein, significantly increases their pandemic risk (11). Animal experiments have further confirmed that these viruses can undergo airborne transmission in ferrets (12–13). Concurrently, other subtypes, including H10N3 and H3N8 viruses, continue to enhance their mammalian adaptability and transmission capacity through key mutations, indicating that the risk posed by strains with pandemic potential cannot be ignored (14-15). These findings collectively underscore the critical importance of early detection and identification of emerging influenza virus strains.

Influenza Pandemic Prevention and Control: Current Progress of Vaccines

During the 2009 H1N1 influenza pandemic, clinical trials were conducted across multiple countries. China's advanced split influenza A virus vaccine demonstrated a protection rate exceeding 85%, with some formulations achieving over 90% efficacy. Although global deployment was delayed, the vaccine's excellent safety profile was subsequently confirmed through surveillance in 70 million recipients and comprehensive post-marketing monitoring, providing critical evidence for worldwide vaccination strategies (16). In response to ongoing pandemic threats and viral evolution, diverse platforms for influenza vaccine research and development have since been established globally, encompassing inactivated, split, attenuated, subunit, adjuvanted, cell culture-based, nucleic acid, and universal influenza vaccines (17–18).

Inactivated influenza vaccines currently represent the most widely deployed vaccine type worldwide. The

inactivation process employs chemicals such as formaldehyde or β-propiolactone to eliminate the virus's replicative capacity and pathogenicity while preserving its antigenic structure (19). Several countries, including China and the United States, have approved inactivated H5N1 subtype pandemic vaccines — China's SFDA granted approval in 2008, while the U.S. FDA approved formulations in 2007 and 2020. However, because these vaccines target previously circulating epidemic strains, regular updates to vaccine components are essential to maintain protective efficacy (20). Live attenuated influenza vaccines (LAIVs) utilize weakened influenza viruses that retain the ability to infect the respiratory mucosa without causing disease (21). Currently, no LAIVs have received approval for pandemic use. Recombinant protein vaccines represent an actively developing platform, produced by expressing specific influenza virus antigens — such as the HA protein — in heterologous expression systems including bacteria, yeast, or insect cells (22).

Notable progress has been achieved in novel vaccine platforms. Nucleic acid vaccines, encompassing both mRNA and DNA vaccines, offer the advantage of rapid development and production once the genetic sequence of the target virus is identified. These vaccines can be engineered to target multiple influenza strains simultaneously, potentially providing broader protection. They also eliminate the need for live virus in production, thereby simplifying the manufacturing process and reducing associated safety concerns (23). countries have initiated research Several development of novel pandemic influenza vaccines for humans, with some vaccines approved to enter clinical trial stages and others receiving emergency use or conditional market approval. For example, the nanoparticle vaccine H5-MNP in Switzerland and the DNA vaccine pVAX-H5 in Russia are currently in the preclinical research stage (24-25); the self-amplifying mRNA H5N1 vaccine in Australia has entered Phase I clinical trials (26); and the mRNA-1018 (H7 and H5) in the United States, along with a codon-optimized mRNA influenza A(H5N1) prepandemic vaccine candidate, have advanced to Phase I/II clinical trials (27-28). In recent years, advances in bioinformatics and artificial intelligence have substantially accelerated the development of pandemic vaccine technology platforms.

China has demonstrated a transition from technology adoption to independent innovation in influenza vaccine research and development, providing valuable technical solutions and practical experience to global influenza prevention and control efforts. Madin-Darby canine kidney (MDCK) cell-based influenza vaccine technology offers an alternative that circumvents the egg supply limitations during pandemics and avoids potential egg-adaptation mutations associated with traditional egg-based production (29). Currently, nine domestic companies have advanced related cell-based vaccines into clinical trials in China: two have completed Phase I clinical trials, while four others are progressing through Phase I or Phase III clinical trials (Table 1). The advantages of low contamination risk and ease of scale-up production position this technology to facilitate industrial-scale manufacturing of cell culture-based influenza vaccines in China.

In universal vaccine research, most candidates remain in the preclinical stage. The Fluaxe mRNA-LNP vaccine has demonstrated cross-protection in a BALB/c mouse model, inducing strong neutralizing antibodies against H1N1, H3N2, H5N1, H7N9 subtypes, and influenza B Victoria lineage virus strains, with neutralizing titers increasing 4- to 9.6-fold. Notably, the vaccine also elicited cross-neutralizing antibodies against strains not included in the original design, encompassing multiple influenza subtypes (e.g., H2, H6, H8, H11, H13, H15, H16). In challenge experiments, the vaccine conferred 100% protection against lethal doses of H1N1 and influenza B Victoria virus while significantly reducing lung viral loads by up to 180.9-fold (30). Similarly, an epitope-optimized nanoparticle vaccine targeting H9N2, developed in China, successfully elicited high levels of cross-reactive antibodies against 14 H9N2 strains from distinct clades in a BALB/c mouse model. In lethal challenge experiments, this vaccine conferred 100% survival and significantly reduced lung viral loads Furthermore, a chimeric hemagglutinin-based mRNA-LNP vaccine platform has demonstrated the capacity to elicit robust and durable stalk-specific antibody responses in a rhesus macaque model. Following a twodose immunization regimen, the induced serum antibody responses and bone marrow plasma cells persisted for at least 10 and 8 months, respectively. Critically, passive transfer of serum collected from vaccinated macaques conferred effective protection in mice against lethal challenge with heterologous influenza viruses, confirming the functional protective efficacy of the vaccine-induced antibodies (32). Collectively, these data provide compelling preclinical evidence supporting the continued development of universal influenza vaccines.

Core Challenges and Future Directions for Influenza Vaccines

Despite substantial progress in vaccine technology, the development and deployment of influenza vaccines for pandemic scenarios encounter several critical obstacles. First, the extended development and production timelines of traditional vaccines limit their capacity to deliver timely protection during the initial outbreak phase. During the 2009 H1N1 pandemic, for instance, vaccine availability in most countries lagged behind peak transmission, substantially diminishing the preventive impact (42). Second, achieving antigenic concordance between vaccine candidates and circulating viral strains represents a fundamental challenge for pandemic vaccine effectiveness. Current influenza vaccines — predominantly inactivated and live-attenuated formulations — rely on predictions of dominant strains for the upcoming season. When these predictions prove inaccurate, antigenic mismatch occurs, substantially reducing vaccine efficacy (43). Moreover, ongoing viral evolution can cause circulating strains to diverge from stockpiled vaccine strains, further compromising protective immunity. Even advanced platforms such as mRNA vaccines remain susceptible to this antigenic mismatch (44). Consequently, exploiting conserved viral antigens to engineer a universal influenza vaccine capable of conferring broad cross-subtype protection has emerged as a pivotal strategy for transcending the inherent limitations of strain-specific vaccine approaches. The successful development of such universal vaccines would facilitate advanced manufacturing and strategic stockpiling, thereby strengthening global pandemic preparedness infrastructure.

Although universal influenza vaccines demonstrate considerable potential for overcoming the limitations of traditional vaccines, no significant breakthrough has been achieved over the past two decades, and their development continues to face substantial challenges. First, universal vaccines target conserved viral antigens such as the HA stalk, M2 ectodomain (M2e), nucleoprotein (NP), and NA, which typically elicit relatively weak protective immune responses (45). Adjuvant development has emerged as a major research focus to overcome this bottleneck. However, adjuvant strategies introduce their own complexities. Adjuvant mechanisms are highly diverse and intricate, necessitating extensive experimental screening to identify optimal combinations with specific antigens. Furthermore, while adjuvants enhance immunogenicity, their potential safety risks must be rigorously controlled, imposing stringent demands on

TABLE 1. Cell-based influenza vaccines in clinical development in China.

Institution	Vaccine	Clinical phase	Target population	Study design	Registration or acceptance ID
Shanghai Institute of Biological Products	Quadrivalent influenza split vaccine (MDCK cells)	Phase I (completed)) ≥6 months	Randomized, double-blind, controlled	CTR20241054 (33)
Changchun Institute of Biological Products	Quadrivalent influenza subunit vaccine (MDCK cells)	e Phase I (Completed) ≥3 years	Randomized, double-blind, controlled	CTR20241413 ((34)
Wuhan Institute of Biological Products	Quadrivalent influenza split vaccine (MDCK cells)	Phase III	≥3 years	Randomized, double-blind, controlled	CTR20233159 (35)
Tianyuan Bio-Pharma	Quadrivalent influenza split vaccine (MDCK cells)	Phase I	≥6 months	Randomized, double-blind, controlled	CTR20240729 (36)
Chengdu Olymvax, Chengdu Xinnuoming, and	Quadrivalent influenza split vaccine (MDCK cells)	Phase I	≥6 months	Randomized, double-blind, controlled Randomized,	Phase I CTR20250319 (37) Phase III: CTR20254267 (38)
Lanzhou Bailing Biotechnology Co., Ltd.	Trivalent influenza split vaccine (MDCK cells)	Phase I	≥6 months	double-blind, controlled	CTR20250309 (39)
Shenzhen Kangtai Biological Products Co.,	Quadrivalent influenza split vaccine (MDCK cells)	Clinical trial approval	≥6 months	Randomized, double-blind, controlled	CXSL2400449 (40)
Ltd. & Lanzhou Bailing Biotechnology Co., Ltd.	Trivalent influenza split vaccine (MDCK cells)	Clinical trial implied permission	≥3 years	Randomized, double-blind, controlled	CXSL2500428 (40)
National vaccine and serum institute	Quadrivalent influenza split vaccine (MDCK cells)	Clinical trial implied permission	-	-	CXSL2300148 (40)
AIM Vaccine Co., Ltd.	Quadrivalent influenza split vaccine (MDCK cells)	Clinical trial implied permission	_	-	CXSL2400629 (40)
Shenzhen Kangtai Biological Products Co.	Quadrivalent influenza split vaccine (MDCK cells)	Phase I	≥6 months	Randomized, double-blind, controlled	CTR20254299 (41)

Note: "-" represents missing data.

Abbreviation: MDCK=madin-darby canine kidney.

rational adjuvant design (46). Consequently, adjuvant technology represents not merely a solution but also a critical bottleneck in universal influenza vaccine development. Second, vaccine efficacy assessment systems require urgent updating. Traditional influenza vaccines rely on neutralizing antibody titers as correlates of protection, whereas universal vaccines may depend more heavily on T-cell immunity or on nonneutralizing antibodies (36). This shift toward new immunological testing paradigms necessitates the development of novel immune correlates and efficacy benchmarks, which pose significant regulatory and clinical challenges. Third, the breadth of protection remains limited. Multi-target strategies that combine conserved internal antigens (e.g., NP) with optimized surface proteins (e.g., the HA stalk) are therefore imperative to broaden the protective spectrum (21). Finally, large-scale production processes for novel vaccine platforms, including messenger RNA (mRNA) virus-like particles (VLPs), underdeveloped. Given these multifaceted challenges, universal influenza vaccines will only fulfill their potential following systematic advances in antigen

design, adjuvant technology, evaluation criteria, and manufacturing capabilities (47). Until such progress is achieved, the timely updating of vaccine strains in response to viral evolution remains the cornerstone of effective influenza immunization.

Summary

Vaccine technology has undergone a transformative evolution — from the complete absence of viral vaccines during the 1918 pandemic to the rapid deployment achieved during the 2009 H1N1 outbreak and subsequent innovations. These technological advances, combined with the global influenza surveillance network, have positioned the international community more strategically than ever to combat future influenza pandemics. Nevertheless, we face substantial challenges in translating this technological potential into effective prevention and control capabilities. Critical issues regarding the immunogenicity, evaluation systems, and production processes of universal vaccines remain unresolved.

Moreover, vaccines alone cannot terminate outbreaks. Their effectiveness depends on sustained viral surveillance and integration within a comprehensive strategy that encompasses antivirals and nonpharmaceutical interventions (NPIs). demonstrates that NPIs — including mask-wearing, social distancing, and public space disinfection — that were implemented during the COVID-19 pandemic resulted in a 46.3% reduction in global influenza cases during the 2020-2021 winter season (48). However, following the relaxation of these measures, influenza activity rebounded dramatically, increasing by 131.7% in winter and 161.2% in summer (48). These empirical observations highlight the critical importance of integrating NPIs with influenza vaccination programs: during the initial emergence of novel influenza strains or periods when vaccines remain unavailable, NPIs function as an essential barrier to slow transmission and provide crucial time for vaccine development and deployment. Once vaccines become widely accessible, NPIs continue to serve a vital complementary role by addressing gaps in vaccineinduced protection, thereby collectively strengthening immune defense systems. Furthermore, emergency vaccine supply capabilities must be enhanced by leveraging established industrial platforms for seasonal influenza vaccines to enable rapid production of pandemic influenza vaccines.

To prepare for future influenza pandemics, a comprehensive strategy must be implemented across three critical domains. First, global influenza surveillance networks require continuous strengthening to ensure the collection of accurate etiological data that supports evidence-based vaccine strain selection. China's national influenza surveillance network exemplifies this approach, encompassing 1,041 sentinel hospitals and 665 network laboratories that collectively test over one million samples annually through virus isolation and deep sequencing, thereby establishing a robust foundation for influenza prevention and control. Second, targeted research must address fundamental technical barriers in universal vaccine development, particularly those related to conserved antigen immunogenicity and scalable manufacturing processes, with the ultimate goal of eliminating dependence on strain prediction. Third, a coordinated framework that integrates vaccination programs with complementary interventions — specifically antiviral therapeutics and non-pharmaceutical measures must be optimized to establish multilayered pandemic defense capabilities. Only through achieving synergistic integration of surveillance systems, vaccine research and development, and comprehensive control measures can we adequately prepare for the next influenza pandemic.

Conflicts of interest: No conflicts of interest.

Funding: Supported by the National Key Research and Development Program of China (grant number 2022YFC2303800).

doi: 10.46234/ccdcw2025.231

Copyright © 2025 by Chinese Center for Disease Control and Prevention. All content is distributed under a Creative Commons Attribution Non Commercial License 4.0 (CC BY-NC).

Submitted: October 13, 2025 Accepted: October 26, 2025 Issued: October 31, 2025

REFERENCES

- Keilman LJ. Seasonal influenza (flu). Nurs Clin N Am 2019;54(2): 227 – 43. https://doi.org/10.1016/j.cnur.2019.02.009.
- Nypaver C, Dehlinger C, Carter C. Influenza and influenza vaccine: a review. J Midwifery Wom Heal 2021;66(1):45 – 53. https://doi.org/10. 1111/jmwh.13203.
- Mokalla VR, Gundarapu S, Kaushik RS, Rajput M, Tummala H. Influenza vaccines: current status, adjuvant strategies, and efficacy. Vaccines 2025;13(9):962. https://doi.org/10.3390/vaccines13090962.
- 4. Neumann G, Kawaoka Y. Which virus will cause the next pandemic? Viruses 2023;15(1):199. http://dx.doi.org/10.3390/v15010199.
- Shi JZ, Zeng XY, Cui PF, Yan C, Chen HL. Alarming situation of emerging H5 and H7 avian influenza and effective control strategies. Emerg Microbes Infec 2023;12(1):2155072. https://doi.org/10.1080/ 22221751.2022.2155072.
- Li CJ, Chen HL. H7N9 influenza virus in China. Cold Spring Harb Perspect Med 2021;11(8):a038349. https://doi.org/10.1101/ cshperspect.a038349.
- Wang L, Gao GF. A brief history of human infections with H5Ny avian influenza viruses. Cell Host Microbe 2025;33(2):176 – 81. https://doi. org/10.1016/j.chom.2025.01.010.
- 8. World Health Organization. Cumulative number of confirmed human cases for avian influenza A(H5N1) reported to WHO, 2003-2023. Geneva: World Health Organization; 2023. https://www.who.int/publications/m/item/cumulative-number-of-confirmed-human-casesfor-avian-influenza-a(h5n1)-reported-to-who--2003-2023--3-october-2023
- 9. Plaza PI, Gamarra-Toledo V, Euguí JR, Lambertucci SA. Recent changes in patterns of mammal infection with highly pathogenic avian influenza A(H5N1) virus worldwide. Emerg Infect Dis 2024;30(3):444 52. https://doi.org/10.3201/eid3003.231098.
- Shi JZ, Kong HH, Cui PF, Deng GH, Zeng XY, Jiang YP, et al. H5N1 virus invades the mammary glands of dairy cattle through 'mouth-to-teat' transmission. Natl Sci Rev 2025;12(9):nwaf262. https://doi.org/10.1093/nsr/nwaf262.
- Marchenko VY, Panova AS, Kolosova NP, Gudymo AS, Svyatchenko SV, Danilenko AV, et al. Characterization of H5N1 avian influenza virus isolated from bird in Russia with the E627K mutation in the PB2 protein. Sci Rep 2024;14(1):26490. https://doi.org/10.1038/s41598-024-78175-y.
- 12. Xiong JL, Ding SP, Zhou JT, Cui YQ, Chen XN, Huang LH, et al. Clade 2. 3.4.4b highly pathogenic H5N1 influenza viruses from birds

^{*} Corresponding author: Dayan Wang, wangdayan@ivdc.chinacdc.cn.

¹ National Key Laboratory of Intelligent Tracking and Forecasting for Infectious Disease, National Institute for Viral Disease Control and Prevention, Chinese Center for Disease Control and Prevention, Beijing, China.

- in China replicate effectively in bovine cells and pose potential public health risk. Emerg Microbes Infec 2025;14(1):2505649. https://doi.org/10.1080/22221751.2025.2505649.
- Elsmo EJ, Wunschmann A, Beckmen KB, Broughton-Neiswanger LE, Buckles EL, Ellis J, et al. Highly pathogenic avian influenza A(H5N1) virus clade 2.3.4.4b infections in wild terrestrial mammals, United States, 2022. Emerg Infect Dis 2023;29(12):2451-60. http://dx.doi.org/ 10.3201/eid2912.230464.
- Yang JY, Zhang Y, Yang L, Li XY, Bo H, Liu J, et al. Evolution of avian influenza virus (H3) with spillover into humans, China. Emerg Infect Dis 2023;29(6):1191 – 201. https://doi.org/10.3201/eid2906.221786.
- Zhu WF, Yang L, Han X, Tan M, Zou SM, Li XY, et al. Origin, pathogenicity, and transmissibility of a human isolated influenza A (H10N3) virus from China. Emerg Microbes Infec 2025;14(1): 2432364. https://doi.org/10.1080/22221751.2024.2432364.
- Shi JR, Shen AL, Cheng Y, Zhang C, Yang XM. 30-year development of inactivated virus vaccine in China. Pharmaceutics 2023;15(12):2721. https://doi.org/10.3390/pharmaceutics15122721.
- Zhang JY, Nian XX, Li XD, Huang SH, Duan K, Li XG, et al. The epidemiology of influenza and the associated vaccines development in China: a review. Vaccines 2022;10(11):1873. https://doi.org/10.3390/ vaccines10111873.
- Information on the delivery of pharmaceutical approval certification documents (October 10, 2025). National Medical Products Administration; 2025. https://www.nmpa.gov.cn/zwfw/sdxx/sdxxyp/ yppjfb/20251010153004185.html.
- Shi H, Ross TM. Inactivated recombinant influenza vaccine: the promising direction for the next generation of influenza vaccine. Expert Rev Vaccines 2024;23(1):409 – 18. https://doi.org/10.1080/14760584. 2024.2333338.
- Xu H, Zhu SY, Govinden R, Chenia HY. Multiple vaccines and strategies for pandemic preparedness of avian influenza virus. Viruses 2023;15(8):1694. https://doi.org/10.3390/v15081694.
- Parvez S, Pathrathota A, Uppar AL, Yadagiri G, Mudavath SL. Influenza virus: global health impact, strategies, challenges, role of nanotechnolgy in influenza vaccine development. Vaccines 2025;13(9): 890. https://doi.org/10.3390/vaccines13090890.
- Khudainazarova NS, Granovskiy DL, Kondakova OA, Ryabchevskaya EM, Kovalenko AO, Evtushenko EA, et al. Prokaryote- and eukaryote-based expression systems: advances in post-pandemic viral antigen production for vaccines. Int J Mol Sci 2024;25(22):11979. https://doi.org/10.3390/ijms252211979.
- Chen JJ, Chen JZ, Xu QB. Current developments and challenges of mRNA vaccines. Annu Rev Biomed Eng 2022;24:85 – 109. https://doi. org/10.1146/annurev-bioeng-110220-031722.
- 24. Rudometov AP, Litvinova VR, Gudymo AS, Ivanova KI, Rudometova NB, Kisakov DN, et al. Dose-dependent effect of DNA vaccine pVAX-H5 encoding a modified hemagglutinin of influenza A (H5N8) and its cross-reactivity against A (H5N1) influenza viruses of clade 2. 3.4.4b. Viruses 2025;17(3):330. https://doi.org/10.3390/v17030330.
- Patel N, Rehman A, Trost JF, Flores R, Longacre Z, Guebre-Xabier M, et al. Single-dose avian influenza A(H5N1) clade 2. 3.4.4b hemagglutinin-Matrix-M* nanoparticle vaccine induces neutralizing responses in nonhuman primates. Nat Commun 2025;16(1):6625. https://doi.org/10.1038/s41467-025-61964-y.
- 26. CTV. Safety, reactogenicity, and immunogenicity study of a self-amplifying mRNA influenza vaccine in healthy adults. 2025. https://ctv.veeva.com/study/safety-reactogenicity-and-immunogenicity-study-of-a-self-amplifying-mrna-influenza-vaccine-in-heal. [2025-10-10].
- CTV. A study of mRNA-1018 pandemic influenza candidate vaccines in healthy adults. 2025. https://ctv.veeva.com/study/a-study-of-mrna-1018-pandemic-influenza-candidate-vaccines-in-healthy-adults. [2025-10-10].
- 28. A study to find and confirm the dose and assess safety, reactogenicity and immune response of a vaccine against pandemic H5N1 influenza virus in healthy younger and older adults. 2025. https://trial.medpath.com/clinical-trial/6af52e87e7b65ce9/nct06382311-randomized-observer-blind-dose-finding-dose-confirmation-mrna-based-pandemic. [2025-10-10].
- 29. Hardenberg G, Brouwer C, van Gemerden R, Jones NJ, Marriott AC,

- Rip J. Polymeric nanoparticle-based mRNA vaccine is protective against influenza virus infection in ferrets. Mol Ther Nucl Acids 2024;35(1): 102159. https://doi.org/10.1016/j.omtn.2024.102159.
- Yi DR, Liu Q, Guo SS, Li QJ, Zhang YX, Li N, et al. Chimeric hemagglutinin and M2 mRNA vaccine for broad influenza subtype protection. npj Vaccines 2025;10(1):113. https://doi.org/10.1038/ s41541-025-01178-x.
- 31. Hao MC, Wang YH, Yang WX, Xu M, Guan YW, Zhang Y, et al. Epitope-optimized influenza hemagglutinin nanoparticle vaccine provides broad cross-reactive immunity against H9N2 influenza virus. ACS Nano 2025;19(22):20824 40. https://doi.org/10.1021/acsnano. 5c03199.
- 32. Styles TM, Akhtar A, Gu CY, Neumann G, Muramatsu H, McPartlan JS, et al. Chimeric hemagglutinin-based universal influenza mRNA vaccine induces protective immunity and bone marrow plasma cells in rhesus macaques. Cell Rep Med 2025;6(10):102369. https://doi.org/10.1016/j.xcrm.2025.102369.
- Center For Drug Evaluation. Detailed information of CTR20241054. http://www.chinadrugtrials.org.cn/clinicaltrials.searchlistdetail.dhtml.
- Center For Drug Evaluation. Detailed infoormation of CTR20241413.
 2024. http://www.chinadrugtrials.org.cn/clinicaltrials.searchlistdetail.
 dhtml
- Center for Drug Evaluation. Detailed information of CTR20233159.
 http://www.chinadrugtrials.org.cn/clinicaltrials.searchlistdetail. dhtml?id=743a5631d4df4fd5a296777c87db0f1c. [2025-10-10].(In Chinese).
- 36. Center for Drug Evaluation. Detailed information of CTR20240729. 2023. https://www.yscro.com/index.php/cde/313ad820a3b87848355b390ce7c0c9ba.html. [2025-10-10]. (In Chinese).
- Center for Drug Evaluation. Detailed information of CTR20250319.
 https://www.yscro.com/index.php/cde/87dd818ebf96472d8b 486d3cee6f6d79.html.[2025-10-10]. (In Chinese).
- Center For Drug Evaluation. Detailed information of CTR20254267.
 http://www.chinadrugtrials.org.cn/clinicaltrials.searchlistdetail.
- Center for Drug Evaluation. Detailed information of CTR20250309.
 http://www.chinadrugtrials.org.cn/clinicaltrials.searchlistdetail. dhtml?id=d06ff57863454e2dbd871b726768b746. [2025-10-10].(In Chinese).
- Center for Drug Evaluation. Drug Clinical Trial Registration and Information Disclosure. 2024. https://www.cde.org.cn/main/xxgk/ listpage/9f9c74c73e0f8f56a8bfbc646055026d.
- Center for Drug Evaluation. Detailed information of CTR20254229.
 http://www.chinadrugtrials.org.cn/clinicaltrials.searchlistdetail. dhtml. (In Chinese).
- Wang DY, Shu YL. History and reflection of pandemic influenza. Sci Sin Vitae 2018;48(12):1247 – 51. https://doi.org/10.1360/N052018-00205.
- 43. Roepke KC, Howard KP. Conformation and membrane topology of the N-terminal ectodomain of influenza A M2 protein. Membranes 2025;15(2):40. https://doi.org/10.3390/membranes15020040.
- 44. Kim H, Webster RG, Webby RJ. Influenza virus: dealing with a drifting and shifting pathogen. Viral Immunol 2018;31(2):174 83. https://doi.org/10.1089/vim.2017.0141.
- 45. Wang WC, Sayedahmed EE, Sambhara S, Mittal SK. Progress towards the development of a universal influenza vaccine. Viruses 2022;14(8): 1684. https://doi.org/10.3390/v14081684.
- Facciolà A, Visalli G, Laganà A, Di Pietro A. An overview of vaccine adjuvants: current evidence and future perspectives. Vaccines 2022;10 (5):819. https://doi.org/10.3390/vaccines10050819.
- 47. Taaffe J, Ostrowsky JT, Mott J, Goldin S, Friede M, Gsell P, et al. Advancing influenza vaccines: a review of next-generation candidates and their potential for global health impact. Vaccine 2024;42(26): 126408. https://doi.org/10.1016/j.vaccine.2024.126408.
- 48. Chen L, Guo YC, López-Güell K, Ma J, Dong YH, Xie JQ, et al. Immunity debt for seasonal influenza after the COVID-19 pandemic and as a result of nonpharmaceutical interventions: an ecological analysis and cohort study. Adv Sci 2025;12(20):2410513. https://doi.org/10.1002/advs.202410513.

Preplanned Studies

Epidemiological Assessment and Optimization of School-Based Influenza Vaccination — Shenzhen City, Guangdong Province, China, 2023–2024

Shuqi Wang^{1,2,3,&}; Zhigao Chen^{4,&}; Qi Tan⁵; Zengyang Shao^{1,3}; Yushuang Chen^{1,3}; Fang Huang⁴; Yanpeng Cheng⁴; Jianxing Yu⁶; Ting Zhang⁶; Xin Wang⁴; Xiujuan Tang^{4,#}; Zhen Zhang⁴; Chao Gao^{7,#}; Zhongjie Li^{6,#}; Zhanwei Du^{8,9}

Summary

What is already known about this topic?

School-aged children represent a particularly vulnerable population for influenza transmission due to their dense social interactions and limited awareness of protective measures. Since 2019, Shenzhen has provided free influenza immunizations to this demographic, with vaccination campaigns typically initiated during the autumn months.

What is added by this report?

This study utilized influenza surveillance data from Shenzhen to develop an age-stratified compartmental model for epidemiological simulations, evaluating the disease burden prevented by influenza vaccinations among school-aged children during the 2023–2024 season. Additionally, an optimization framework was developed to design strategic vaccination schedules while considering the importance of maintaining stable public health policies over time.

What are the implications for public health practice?

The findings suggest concentrating vaccination efforts during November and December; however, optimal strategies may vary depending on specific influenza transmission patterns. A more robust approach involves implementing a generalized strategy optimized using historical seasonal data with comparable transmission characteristics.

ABSTRACT

Introduction: School-aged children are primary vectors for influenza transmission through their frequent close contact in educational settings and developing immune awareness. Since 2019, the Shenzhen municipal government has implemented annual, free, influenza vaccination programs targeting

eligible primary and secondary school students. However, evidence-based strategies specifically tailored to this demographic remain insufficient.

Methods: This study analyzed weekly influenza-like illness (ILI) surveillance data and laboratory-confirmed positivity rates from Shenzhen during the 2023–2024 season. It developed an age-stratified Susceptible—Exposed—Symptomatic—Asymptomatic—Recovered—Hospitalized—Deceased—Vaccinated compartmental model integrated with the Ensemble Adjustment Kalman Filter (EAKF) algorithm to estimate historical transmission parameters and quantify vaccination impact. The Upper Confidence Bound applied to Trees (UCT) algorithm was used to optimize the vaccination schedule and evaluate multiple strategic scenarios comparatively.

Results: Compared to a no-vaccination scenario, the current government strategy prevented approximately 1,285,925 [95% confidence interval 1,240,671-1,331,180] symptomatic infections and 56,956 (95% *CI*: 55,118–58,793) hospitalizations. Under identical vaccine supply conditions, the optimized strategy recommends vaccinating 30%, 25%, and 5% of school-aged children in November, December, and January, respectively. This optimized approach would avert approximately 1,469,368 (95% CI: 1,392,734–1,546,002) symptomatic infections and 64,442 (95% CI: 61,269-67,615) hospitalizations representing 14.3% and 13.1% improvements over the government strategy, respectively. Additionally, a generic strategy developed using 2017-2019 data performed well during 2023-2024, demonstrating cross-seasonal adaptability.

Conclusions: Concentrating influenza vaccination efforts among school-enrolled children during November and December significantly reduces disease burden and represents a critical strategy for controlling influenza transmission.

Influenza represents a significant acute respiratory infectious disease that poses substantial public health worldwide. Educational institutions, characterized by dense student populations, limited mobility patterns, and frequent close interpersonal contact, constitute particularly high-risk environments for influenza transmission and outbreaks (1). Schoolaged children demonstrate heightened susceptibility to viral infection compared to adults and, once infected, typically exhibit prolonged viral shedding periods with higher viral loads (2). These epidemiological characteristics underscore the critical importance of implementing targeted, evidence-based countermeasures within school settings. Among available pharmaceutical interventions, vaccination remains the most effective strategy for preventing influenza-related infections (3).

Since 2019, Shenzhen's vaccination program has provided free influenza vaccinations to school-aged typically implementing these programs during October and November each year. Despite influenza extensive research vaccination on optimization strategies (4-5), the evidence base supporting vaccination decisions for this specific population remains limited, creating a gap between recommendations theoretical and practical implementation for school-based programs.

To assess the epidemiological impact of school-based vaccination programs, this study analyzed influenza transmission patterns in Shenzhen during the 2023-2024 season and compared observed outcomes with simulated scenarios assuming no vaccination intervention. This study utilized weekly ILI+ proxy data spanning August 2023 to July 2024, along with vaccination coverage data provided by the Shenzhen Center for Disease Control and Prevention (CDC), to estimate reductions in infections and hospitalizations attributable to vaccination (Supplementary Material and Supplementary Figure S1, available at https:// weekly.chinacdc.cn/). The ILI+ proxy integrates influenza-like illness (ILI) rates with laboratoryconfirmed positivity rates, providing a comprehensive measure of influenza activity that captures both clinical presentation and virological confirmation. reconstruct historical influenza transmission dynamics, this study implemented an age-specific Susceptible -Exposed – Symptomatic – Asymptomatic – Recovered – Hospitalized – Deceased – Vaccinated (SEYARHDV) compartmental model, which effectively characterizes viral spread across different population segments (Supplementary Material, Supplementary Figure S2,

and Supplementary Table S1, available at https:// weekly.chinacdc.cn/). By coupling this transmission model with the Ensemble Adjustment Kalman Filter (EAKF) algorithm (6), this study estimated timevarying transmission rates and other epidemiological parameters to quantify the public health impact of vaccination programs, specifically measuring reductions in symptomatic infections and hospitalizations (Supplementary Material).

For the optimization process, this study employed the Upper Confidence Bound applied to Trees (UCT) algorithm to identify an optimal vaccination schedule for school-aged children (Supplementary Material) (7). To address implementation challenges such as dispersed vaccination timing and uneven distribution patterns, it introduced a smoothness constraint to ensure gradual policy rollout and prevent abrupt strategic shifts. The optimization framework begins each September — coinciding with the academic year commencement — and spans a 12-month period with monthly decision intervals, aiming to minimize annual influenza-related hospitalizations. Based on the vaccination strategy implemented by the Shenzhen government, as documented by the Shenzhen CDC for 2023-2024, this study established an annual vaccination rate of 60% for children aged 6-18 years. Each month offers 6 vaccination options: 0%, 5%, 10%, 25%, 30%, or 45%, permitting up to 45% of school-aged children to receive vaccination monthly. For other age groups (0–5 years, 19–59 years, and \geq 60 years), monthly and annual vaccination rates align with actual vaccination data from 2023 to 2024. Under the baseline strategy — where annual vaccination rates are distributed evenly across months — school-aged children receive a consistent monthly vaccination rate of 5%, while other groups maintain their default Vaccines are administered throughout each day. Additional experimental details are provided in Supplementary Material.

For the 2023–2024 period, this study fitted the SEYARHDV model and found that the influenza season extended from September 2023 to May 2024, with a peak ILI+ proxy of 0.0665 (Figure 1A). In a simulated scenario without vaccination, the projected peak ILI+ proxy increased dramatically to 0.2728, demonstrating the critical importance of vaccination in epidemic control. The Shenzhen vaccination program prevented approximately 1,285,925 (95% *CI*: 1,240,671–1,331,180) symptomatic infections and 56,956 (95% *CI*: 55,118–58,793) hospitalizations in 2023–2024. By comparison, the baseline vaccination

strategy prevented only 704,669 (95% CI: 669,089-740,249) symptomatic infections and 32,175 30,641–33,709) hospitalizations, demonstrating substantially lower effectiveness than the government's approach. Using the same vaccine supply, optimized strategy recommended vaccinating 30%, 25%, and 5% of school-aged children in November, December, and January, respectively. This optimized approach could prevent 1,469,368 (95% CI: 1,392,734–1,546,002) symptomatic infections and 64,442 (95% CI: 61,269-67,615) hospitalizations. Compared to the government's vaccination strategy, the optimized approach achieved a 14.3% greater reduction in symptomatic infections and a 13.1% greater reduction in hospitalizations, demonstrating superior effectiveness in controlling influenza transmission.

Figure 1B illustrates the differences in ILI+ proxy trends across vaccination strategies. Similar analyses were conducted using 2017–2019 data, with results provided in Supplementary Material and Supplementary Figure S3 (available at https://weekly.chinacdc.cn/).

To develop a vaccination strategy applicable to future influenza seasons, this study sought to derive an optimal approach using historical data that could be applied to prospective scenarios. It optimized vaccination strategies for the 2017–2018 and 2018–2019 influenza seasons using data from 2017 to 2019 (Supplementary Material). A comprehensive, universal strategy was obtained by calculating a weighted average of the optimization results from these two seasons, which recommended vaccinating 15% and 45% of school-aged children in October and

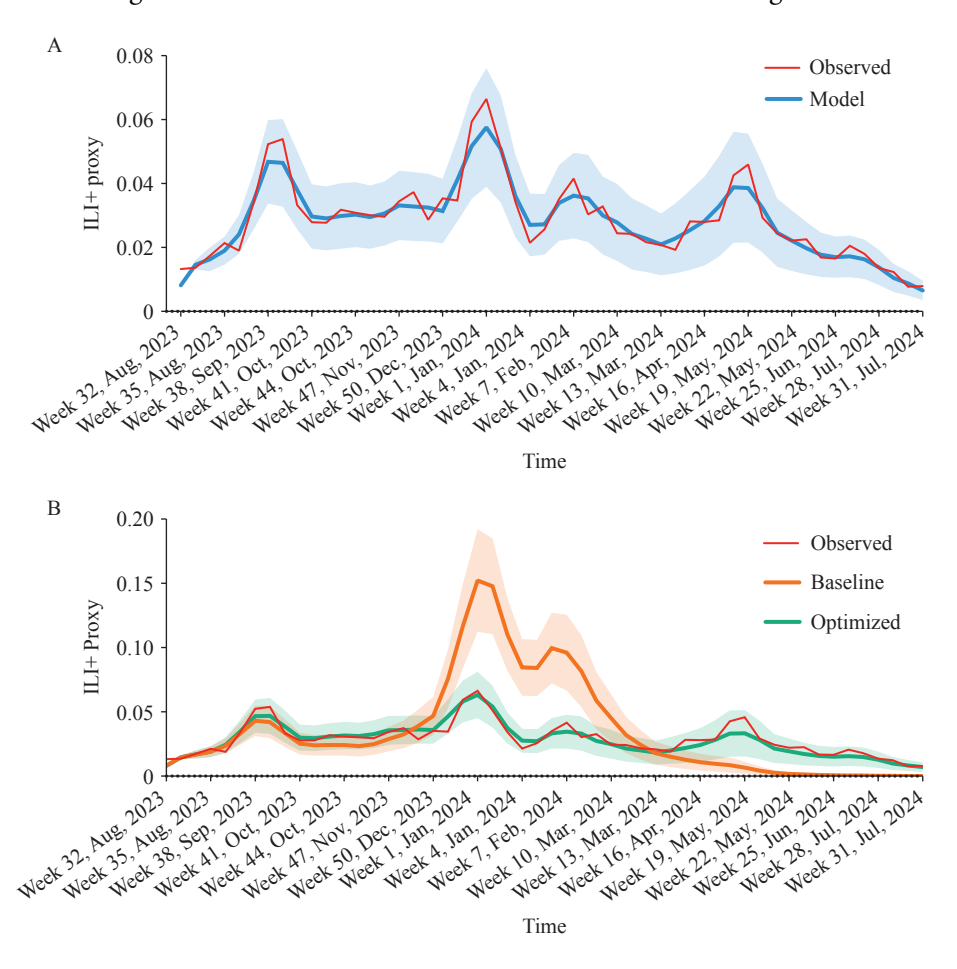


FIGURE 1. Model fitting and simulation of influenza activity under different vaccination strategies, Shenzhen, 2023–2024. (A) Observed ILI+ proxy from surveillance data (red) and corresponding model fitting results (blue line with shaded 95% *CI*). (B) Comparison of observed ILI+ (red) with model-simulated outcomes under two strategies: baseline (orange) and optimized (green), shown as lines with shaded 95% *CI*s.

Note: All scenarios assume the same annual vaccine coverage. For school-aged children, only the monthly distribution differs; other age groups follow actual 2023–2024 rates.

Abbreviation: C/=confidence interval; ILI+=influenza-positive proportion.

November, respectively. When this strategy was applied to the 2023–2024 influenza season, it potentially reduced symptomatic infections 1,187,407 (95% CI: 1,150,194-1,224,620) and hospitalizations by 52,924 (95% CI: 51,408-54,439). Although this strategy's effectiveness was slightly lower than the government-enforced strategy, demonstrated robust performance, making it suitable vaccination policy recommendations. difference in effectiveness can be attributed to significant variations in transmission patterns across different influenza seasons. For instance, 2017–2018 influenza season was predominantly confined to the winter-spring period with relatively low case numbers, while the 2018-2019 experienced significant outbreaks in both winter-spring and summer periods. In contrast, the 2023-2024 season extended from summer and autumn to the following spring and summer, with a higher overall peak. These findings suggest that future strategy optimization should incorporate more comprehensive historical data and predictions about influenza transmission levels. A universal strategy optimized using data from seasons with similar transmission patterns would likely prove more effective and better suited to adapting to the dynamic nature of influenza transmission.

To better understand how different age groups contribute to the observed vaccination effectiveness, this study conducted additional simulations by sequentially removing vaccination coverage for each age group while maintaining coverage for all others. This approach allowed the quantification of the marginal impact of each age group on overall disease burden during the 2023-2024 season. The results demonstrated that removing vaccination for the 6-18 year group led to the most substantial increase in disease burden, resulting in an estimated 3,823,546 (95% CI: 3,513,522–4,133,570) symptomatic infections and 175,283 (95% CI: 162,422-188,143) hospitalizations — substantially higher than any other age group. In comparison, removing vaccination for the 0-5 year group resulted in 2,679,188 (95% CI: 2,406,184-2,952,192) symptomatic infections and 128,517 (95% CI: 116,848-140,186) hospitalizations. Removing vaccination for the 19-59 year group yielded 2,719,808 (95% CI: 2,444,489-2,995,128) symptomatic infections and 130,408 (95% CI: 118,631-142,185) hospitalizations. Finally, removing vaccination for the ≥60 year group led to 2,677,089 2,404,110–2,950,069) (95% CI: symptomatic infections and 130,414 (95% CI: 118,546–142,282) hospitalizations. These findings highlight that while all age groups contribute to overall protection, the marginal impact of vaccinating school-aged children is notably greater in reducing population-level transmission and disease burden. This result aligns with both theoretical expectations and practical implementation, as the Shenzhen vaccination program has primarily targeted school-aged children and achieved the highest coverage in this demographic.

DISCUSSION

The spread of influenza has created severe health school-aged challenges among children. This demographic faces heightened susceptibility to crossinfection within school environments due to their limited self-protection awareness and frequent close peer interactions (8). Such intensive contact not only facilitates within-school transmission but significantly amplifies community-level spread. Infected children often serve as vectors, carrying the virus into their households and triggering cascading consequences, including parental absenteeism and secondary infections among family members. Research demonstrates that for every 10 students absent from school due to influenza, approximately 8 household members subsequently become ill, with illness rates within 3 days of school absence being 2.2 times higher than expected during the influenza season (9). This evidence confirms that school-aged children frequently serve as primary introducers of influenza into households. Consequently, vaccinating school-aged children not only reduces their individual disease burden but also disrupts transmission pathways between schools and households, helping to curb thereby community-level spread and broader alleviating the overall public health and socioeconomic burden of seasonal influenza.

Although school-aged children are not traditionally considered the primary target of influenza vaccination, many countries now recommend including them in immunization programs as an extension of existing plans (10). This shift reflects growing recognition of their central role in influenza transmission. In Shenzhen, influenza vaccination is available to all individuals aged 6 months and older, with free vaccinations currently accessible only to school-aged children and elderly individuals aged 60 and above. Others who intend to receive vaccinations need to voluntarily visit clinics at their own expense for

preventive immunization. It is worth noting that influenza vaccination for the elderly is also entirely voluntary. Hence, this study investigated the public health benefits of vaccination policies and examined optimal strategies for vaccinating school-aged children. Its findings underscore the importance of vaccination timing and coverage, highlighting the advantages of well-planned public health interventions.

This study has several limitations that should be acknowledged. First, its investigation of vaccination strategies did not consider other interventions such as social distancing measures. Second, this study utilized weekly ILI+ proxy data and healthcare-seeking rates to estimate symptomatic incidence in the general population from municipal-scale data, which may introduce biases in attack rate calculations. Third, this study considered only six possible vaccination actions to balance varying vaccination rates while minimizing computational complexity. It also assumed a maximum monthly vaccination rate of 45%, which constrained this study's action space. Regions can adjust these actions and constraints based on their vaccination capacity and local conditions. Fourth, since unified mass influenza vaccination targets only school-aged children, this study assumed vaccination rates for other age groups remained fixed and focused solely on optimizing the vaccination schedule for school-aged children. However, this methodology can be similarly applied to other regions and age groups.

This study's findings demonstrate that Shenzhen's large-scale, targeted vaccination program for schoolaged children substantially reduces influenza-related disease burden, including both infections and hospitalizations. The optimization algorithm that this study developed provides a valuable framework for refining vaccination strategies across different settings. While vaccination approaches may require adaptation specific influenza transmission patterns, concentrating vaccination efforts during November December consistently proves effective, establishing a robust foundation for future vaccination policies.

Conflicts of interest: No conflicts of interest.

Funding: Supported by the National Key R&D Program of China (2022YFE0112300, 2023YFC2308701), the National Natural Science Foundation of China (82304204), the Natural Science Foundation of Guangdong Province (2025A1515011908), the Technological Innovation Team of Shaanxi Province (2025RS-CXTD-009), the

International Cooperation Project of Shaanxi Province (2025GH-YBXM-017), the Shenzhen-Hong Kong-Macau Science and Technology Project (Category C) (SGDX20230821091559022), the Fundamental Research Funds for the Central Universities (G2024WD0151, D5000240309), and the CAMS Innovation Fund for Medical Sciences (2021-I2M-1-044).

doi: 10.46234/ccdcw2025.232

Copyright © 2025 by Chinese Center for Disease Control and Prevention. All content is distributed under a Creative Commons Attribution Non Commercial License $4.0 \ (CC\ BY-NC)$.

Submitted: July 21, 2025 Accepted: September 25, 2025 Issued: October 31, 2025

REFERENCES

- Shi JH, Xiang NJ, Zhang YP, Chen M, Sun SH, Chen T, et al. Epidemiological characteristics on the clustering nature of pandemic (H1N1) 2009 in China. Chin J Epidemiol 2012;33(1):62 – 6. https://doi.org/10.3760/cma.j.issn.0254-6450.2012.01.014.
- Wu S, Van Asten L, Wang L, McDonald SA, Pan Y, Duan W, et al. Estimated incidence and number of outpatient visits for seasonal influenza in 2015-2016 in Beijing, China. Epidemiol Infect 2017;145 (16):3334 – 44. https://doi.org/10.1017/S0950268817002369.
- 3. Wang Z, Bauch CT, Bhattacharyya S, d'Onofrio A, Manfredi P, Perc M, et al. Statistical physics of vaccination. Phys Rep 2016;664:1 113. https://doi.org/10.1016/j.physrep.2016.10.006.
- Venkatramanan S, Chen JZ, Fadikar A, Gupta S, Higdon D, Lewis B, et al. Optimizing spatial allocation of seasonal influenza vaccine under temporal constraints. PLoS Comput Biol 2019;15(9):e1007111. https://doi.org/10.1371/journal.pcbi.1007111.
- Kahana D, Yamin D. Accounting for the spread of vaccination behavior to optimize influenza vaccination programs. PLoS One 2021;16(6): e0252510. https://doi.org/10.1371/journal.pone.0252510.
- 6. Pei S, Teng X, Lewis P, Shaman J. Optimizing respiratory virus surveillance networks using uncertainty propagation. Nat Commun

[#] Corresponding authors: Xiujuan Tang, txj43@126.com; Chao Gao, cgao@nwpu.edu.cn; Zhongjie Li, lizhongjie@sph.pumc.edu.cn.

WHO Collaborating Centre for Infectious Disease Epidemiology and Control, School of Public Health, Li Ka Shing Faculty of Medicine, University of Hong Kong, Hong Kong Special Administrative Region, ² School of Cybersecurity, Northwestern Polytechnical University, Xi'an City, Shaanxi Province, China; 3 Laboratory of Data Discovery for Health Limited, Hong Kong Science and Technology Park, Hong Kong Special Administrative Region, China; ⁴ Shenzhen Center for Disease Control and Prevention, Shenzhen City, Guangdong Province, China; 5 College of Computer and Information Engineering (College of Artificial Intelligence), Nanjing Tech University, Nanjing City, Jiangsu Province, China; 6 School of Population Medicine and Public Health, Chinese Academy of Medical Sciences & Peking Union Medical College, Beijing, China; School of Artificial Intelligence, Optics, and Electronics (iOPEN), Northwestern Polytechnical University, Xi'an City, Shaanxi Province, China; 8 School of Public Health and Emergency Management, Southern University of Science and Technology, Shenzhen City, Guangdong Province, China; ⁹ School of Medicine, Yunnan University, Kunming City, Yunnan Province, China. & Joint first authors.

China CDC Weekly

- 2021;12(1):222. https://doi.org/10.1038/s41467-020-20399-3.
- Kocsis L, Szepesvári C. Bandit based monte-carlo planning. In: Proceedings of the 17th European conference on machine learning. Berlin, Germany: Springer. 2006; p. 282-93. http://dx.doi.org/10. 1007/11871842_29.
- Uscher-Pines L, Schwartz HL, Ahmed F, Zheteyeva Y, Tamargo Leschitz J, Pillemer F, et al. Feasibility of social distancing practices in US schools to reduce influenza transmission during a pandemic. J Public Health Manag Pract 2020;26(4):357 – 70. https://doi.org/10.
- 1097/PHH.000000000001174.
- Neuzil KM, Hohlbein C, Zhu YW. Illness among schoolchildren during influenza season: effect on school absenteeism, parental absenteeism from work, and secondary illness in families. Arch Pediatr Adolesc Med 2002;156(10):986 – 91. https://doi.org/10.1001/ archpedi.156.10.986.
- Newall AT, Jit M, Beutels P. Economic evaluations of childhood influenza vaccination: a critical review. Pharmacoeconomics 2012;30 (8):647 – 60. https://doi.org/10.2165/11599130-0000000000-00000.

SUPPLEMENTARY MATERIAL

Data Description

The Shenzhen Center for Disease Control and Prevention provided influenza-like illness (ILI) rates and laboratory-confirmed positivity rates for Shenzhen across 2 distinct periods: Week 45 of 2017 to Week 44 of 2019, preceding the implementation of large-scale centralized vaccination policies for school-aged children, and Week 32 of 2023 to Week 31 of 2024, following policy implementation (Supplementary Figure S1). Data from 2019 to 2023 were excluded to eliminate potential confounding effects from the coronavirus disease 2019 pandemic. ILI encompasses patients presenting with acute respiratory infection, fever (≥38 °C), cough, and/or sore throat. The ILI+ proxy represents the proportion of influenza-positive cases among individuals seeking medical care, calculated by multiplying the ILI rate (ILI%) by the laboratory-positive rate. Influenza season onset is identified as the initial period of 3 consecutive weeks during which ILI+ records exceed a specified baseline, defined as the 40th percentile of non-zero ILI+ records. The season concludes when 2 consecutive weeks show ILI+ records falling below this baseline following onset. To exclude transient spikes, only periods where ILI+ records consistently exceed 3 times the baseline are considered part of the influenza season (1).

This study assumed a parameter μ to map weekly ILI+ proxy values to weekly symptomatic incidence rates in the general population. To determine the optimal μ value, we selected values in 0.05 increments within the 0 to 1 range. The optimal μ value was identified by minimizing the mean squared error (MSE) between simulated and observed ILI+ proxy means.

Epidemic Influenza Transmission Model

This study employed an age-specific Susceptible – Exposed – Symptomatic – Asymptomatic – Recovered – Hospitalized – Deceased (SEYARHD) model to conduct retrospective forecasts of multiple influenza seasons (Supplementary Figure S2A). To explore optimal vaccination strategies, we incorporated a Vaccinated state into the model (Supplementary Figure S2B), resulting in the SEYARHDV model with the following equations:

$$S_{t+1,a} = S_{t,a} - \beta_t S_{t,a} \sum_{i=1}^{4} \left(Y_{t,i} + \omega A_{t,i} \right) \varphi_{ai} / \psi_a + p^{RS} R_{t,a} - u_{t,a} \psi_a S_{t,a} / \left(S_{t,a} + A_{t,a} \right) + f^6 V_{t,a}^6$$

$$E_{t+1,a} = E_{t,a} + \beta_t S_{t,a} \sum_{i=1}^{4} \left(Y_{t,i} + \omega A_{t,i} \right) \varphi_{ai} / \psi_a - p^{EYA} E_{t,a} + \beta_t \sum_{j=1}^{6} \left(1 - v^j \right) V_{t,a}^j \sum_{i=1}^{4} \left(Y_{t,i} + \omega A_{t,i} \right) \varphi_{ai} / \psi_a$$

$$Y_{t+1,a} = Y_{t,a} + \sigma p^{EYA} E_{t,a} - p^{YH} Y_{t,a} - p^{YR} Y_{t,a}$$

$$A_{t+1,a} = A_{t,a} + \left(1 - \sigma \right) p^{EYA} E_{t,a} - p^{AR} A_{t,a}$$

$$R_{t+1,a} = R_{t,a} + p^{AR} A_{t,a} + p^{YR} Y_{t,a} + p^{HR} H_{t,a} - p^{RS} R_{t,a}$$

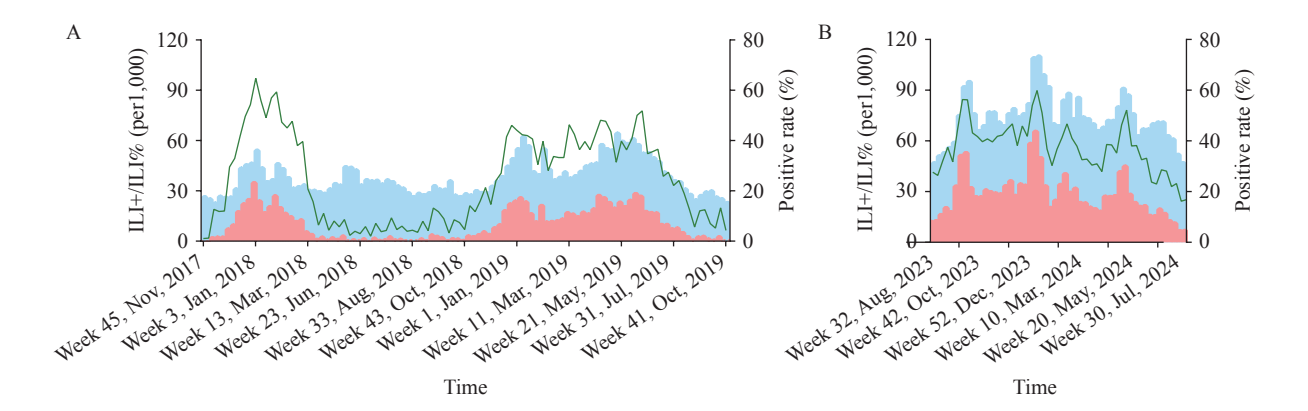
$$H_{t+1,a} = H_{t,a} + p^{YH} Y_{t,a} - p^{HR} H_{t,a} - p^{HD} H_{t,a}$$

$$V_{t+1,a}^1 = V_{t,a}^1 + u_{t,a} \psi_a S_{t,a} / \left(S_{t,a} + A_{t,a} \right) - f^k V_{t,a}^1 - \beta_t \left(1 - v^l \right) V_{t,a}^1 \sum_{i=1}^{4} \left(Y_{t,i} + \omega A_{t,i} \right) \varphi_{ai} / \psi_a$$

$$V_{t+1,a}^k = V_{t,a}^k + f^{k-1} V_{t,a}^{k-1} - f^k V_{t,a}^k - \beta_t \left(1 - v^k \right) V_{t,a}^k \sum_{i=1}^{4} \left(Y_{t,i} + \omega A_{t,i} \right) \varphi_{ai} / \psi_a, \quad k = 2, 3, 4, 5$$

$$V_{t+1,a}^k = V_{t,a}^k + f^k V_{t,a}^k - f^k V_{t,a}^k - \beta_t \left(1 - v^k \right) V_{t,a}^k \sum_{i=1}^{4} \left(Y_{t,i} + \omega A_{t,i} \right) \varphi_{ai} / \psi_a$$

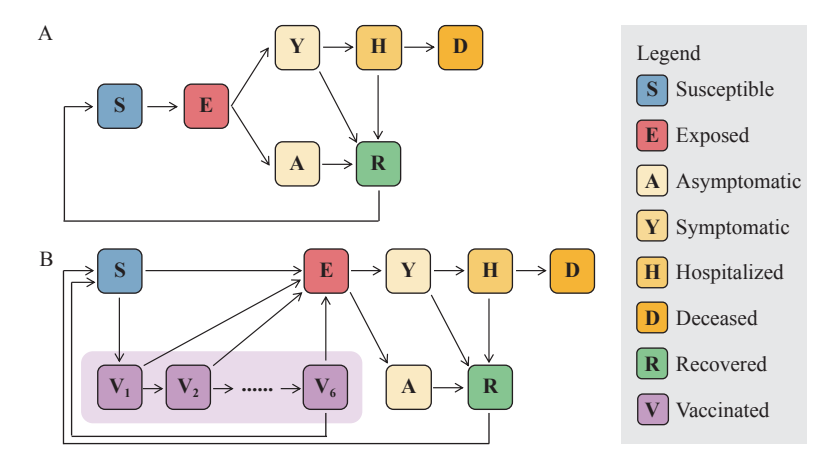
where t represents the time step and a represents age groups (a = 1, 2, 3, 4). S, E, Y, A, R, H, D, and V denote the proportions of the population that are susceptible, exposed, symptomatic infected, asymptomatic infected, recovered, hospitalized, deceased, and vaccinated, respectively. To capture the rise in vaccine efficacy at 1 month followed by a decline at 6 months post-vaccination (2), V is divided into 6 sub-compartments, each with a vaccine efficacy v^k and transition rates between sub-compartments f^k (k = 1, 2, ..., 6). Since asymptomatic individuals exhibit



SUPPLEMENTARY FIGURE S1. Weekly trends of ILI%, laboratory-confirmed positivity rate, and the calculated ILI+ proxy in Shenzhen from (A) 2017 to 2019 and (B) 2023 to 2024.

Note: The red-shaded area represents the ILI+ proxy, the blue-shaded area represents ILI%, and the green curve indicates the laboratory-confirmed positivity rate.

Abbreviation: ILI=influenza-like illness; ILI%=influenza-like illness rate; ILI+=influenza-positive proportion.

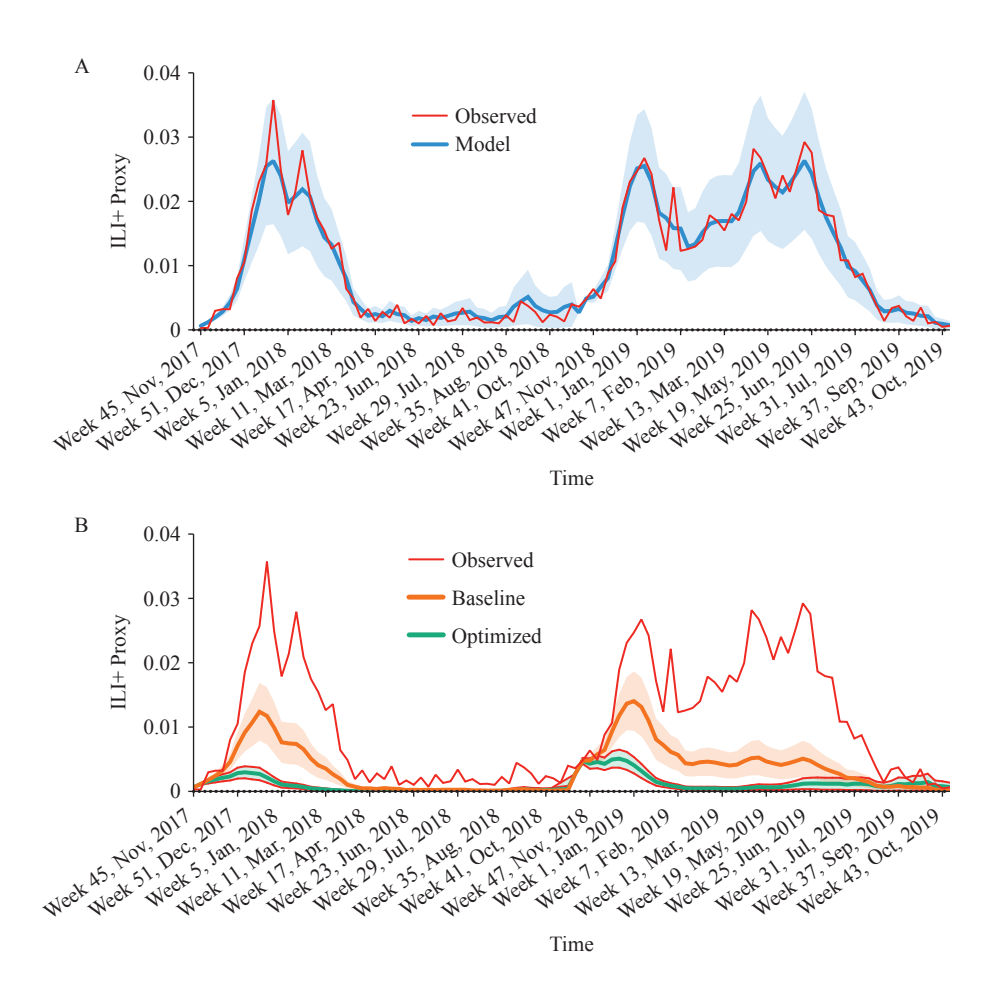


SUPPLEMENTARY FIGURE S2. Schematic representation of the (A) SEYARHD and (B) SEYARHDV epidemiological models for influenza transmission dynamics.

Note: In both frameworks, susceptible individuals transition to an exposed state following infection, where they remain infected but not yet infectious or symptomatic. A proportion of infected cases develop asymptomatic infections with reduced transmissibility before recovering, while the remainder progress to symptomatic illness. Symptomatic individuals subsequently either require hospitalization or recover directly. Hospitalized patients ultimately progress to either recovery or death. Recovered populations gradually return to a susceptible state, maintaining vulnerability to future reinfection. The SEYARHDV model specifically incorporates a vaccinated compartment subdivided into 6 distinct sub-compartments, with protection levels calibrated to estimates reflecting variable vaccine efficacy over time.

Abbreviation: SEYARHD=Susceptible – Exposed – Symptomatic – Asymptomatic – Recovered – Hospitalized – Deceased; SEYARHDV=Susceptible – Exposed – Symptomatic – Asymptomatic – Recovered – Hospitalized – Deceased – Vaccinated.

no symptoms, influenza vaccines may be administered to both susceptible and asymptomatic individuals, though effectiveness is limited to susceptible individuals in preventing infection. $u_{t,a}$ represents the vaccination rate of age group a at time t. β_t indicates the transmission rate at time t, defined as the probability of successful transmission per contact. ϕ_{ai} denotes the average number of contacts an individual in age group a has with age group i. ψ_a represents the population proportion in age group a. ω denotes the relative infectiousness of asymptomatic infections compared to symptomatic infections. σ indicates the proportion of cases that become symptomatic p^{EYA} represents the transition rate from the exposed state; p^{YH} denotes the hospitalization rate of symptomatic cases; p^{YR} , p^{AR} , and p^{HR} represent the recovery rates of symptomatic cases, asymptomatic cases, and hospitalized patients, respectively; p^{HD} represents the mortality rate of hospitalized patients. The specific epidemiological parameter values for the model are presented in Supplementary Table S1.



SUPPLEMENTARY FIGURE S3. Model fitting and simulation of influenza activity under different vaccination strategies, Shenzhen, 2017–2019. (A) Observed ILI+ proxy from surveillance data (red) and corresponding model fitting results (blue line with shaded 95% *CI*). (B) Comparison of observed ILI+ (red) with model-simulated outcomes under two strategies: baseline (orange) and optimized (green), shown as lines with shaded 95% *CIs*.

Note: All scenarios assume identical annual vaccine coverage as implemented in 2023–2024. For school-aged children, only the monthly distribution varies; other age groups maintain actual 2023–2024 vaccination rates. Abbreviation: *CI*=confidence interval; ILI+=influenza-positive proportion.

Ensemble Adjustment Kalman Filter Algorithm

This study employed the highly efficient data assimilation method known as the Ensemble Adjustment Kalman Filter (EAKF) algorithm to estimate weekly transmission rates for historical influenza outbreaks (3–4). The observation and state vectors at time t are denoted as y_t^o and X_t^o , respectively. The state vector is defined as $X_t = (S_{t,1}, E_{t,1}, Y_{t,1}, A_{t,1}, R_{t,1}, H_{t,1}, D_{t,1}, ..., S_{t,4}, E_{t,4}, Y_{t,4}, A_{t,4}, R_{t,4}, H_{t,4}, D_{t,4}, y_t, \beta_t)$, where y_t represents the observed state variable corresponding to symptomatic incidence. In this study's transmission model, weekly symptomatic incidence is calculated as:

$$I_{t} = \sum_{a=1}^{N} \sum_{k=t-6}^{t} \sigma p^{EYA} E_{t,a}$$
 (2)

The EAKF algorithm utilizes an ensemble of particles to represent the posterior distribution of the system state and updates the posterior probability distribution of state X using observations y^o based on Bayesian inference principles. Each particle comprises both a state hypothesis and an associated weight, where the weight indicates the particle's relative contribution to the posterior distribution. During the weight update process, each particle's weight is calculated using a Gaussian likelihood function: $\omega_t^i \propto P(y_t \mid y_t^o, \Omega)$, where $y_t \mid y_t^o$ represents the distance between fitted and observed incidence values, and Ω denotes the variance derived from the standard deviation of the observed incidence vector. These particles undergo resampling according to their weights ω_t^i , which are fitted using

SUPPLEMENTARY TABLE S1. Epidemiological parameters for the influenza transmission model implemented in Shenzhen.

Parameters	Parameter description	Value
N	Total population of Shenzhen	17,681,600 (8)
Ψ	Age-specific population proportions	[0.0566, 0.1314, 0.7584, 0.0535] for [0–5 year, 6–18 year, 19–59 year, ≥60 year] (9)
$\Phi = (\varphi_{ij})$	Contact matrix	[[1.409660734, 1.768548709, 3.751113208, 0.350060933], [0.346000233, 10.64471027, 6.08382839, 0.286702683], [0.570072983, 4.073960628, 10.62071562, 0.482763604], [0.396853292, 1.754034964, 3.745765744, 1.173235326]] for [0–5 year, 6–17 year, 18–59 year, \geq 60 year] (10)
β	Transmission rate	Calibrated
σ	Proportion of infections that are symptomatic	0.55 (11)
ω	Relative infectiousness of asymptomatic infections compared to symptomatic infections	0.36 (11)
$ ho^{RS}$	Transition rate from recovered to susceptible state	1/(4×365) (<i>11</i>)
$ ho^{EYA}$	Transition rate from exposed to symptomatic/asymptomatic state	1/1.5 (12)
p^{AR}	Recovery rate of asymptomatic infections	1/3 (13)
p^{YR}	Recovery rate of symptomatic infections	1/5 ×(1-0.0146) (<i>14</i>)
$oldsymbol{ ho}^{\sf HR}$	Recovery rate of hospitalized patients	0.9981 (11)
$oldsymbol{ ho}^{YH}$	Hospitalization rate	[0.007, 0.0027, 0.0083, 0.0909] for [0–5 year, 6–17 year, 18–59 year, ≥60 year] (11)
$oldsymbol{ ho}^{\sf HD}$	Case fatality rate among hospitalizations	[0.000050, 0.000072, 0.000595, 0.001570] for [0–5 year, 6–17 year, 18–59 year, ≥60 year] (11)
u ^A	Annual vaccination coverage rate	[12%, 55%, 12%, 12%] for [0–5 year, 6–18 yéar, 19–59 year, ≥60 year] (15), with vaccination rates assumed equivalent across all age groups except 6–18 year
V	Vaccine efficacy	[1/2, 9/10, 7/10, 1/2, 3/10, 1/10] for $[V^1, V^2, V^3, V^4, V^5, V^6]$ (2)
f	Transition rate between vaccinated sub-compartments	1/30 (2)
wtp	Willingness of residents to receive influenza vaccines in Shanghai	[0.784, 0.578, 0.730] for [0–18 year, 19–59 year, \geq 60 year] (16)

historical influenza activity data. High-weight particles are retained to ensure that the particle ensemble provides a better approximation of the true posterior distribution.

Retrospective Forecast of Multiple Influenza Seasons

This study reconstructed historical influenza infection patterns in Shenzhen for 2023–2024 using the SEYARHDV model with actual vaccination data incorporated, and for 2017–2019 using the SEYARHD model. During the data assimilation process, we employed Latin Hypercube Sampling (LHS) to draw initial susceptible proportions from a range of [0.65, 0.75], conducting 50 random simulations for each scenario. The weekly incidence rate at time *t*+1 was calculated as the average of these 50 simulation results. In this study, the particle count was set to 10,000. Disease simulations commenced in August (Week 32) for the 2023–2024 period and in November (Week 45) for the 2017–2019 period, approximately one month before the typical onset of each annual influenza season.

Optimization Method

This study integrated a rapid, scalable, and adaptable optimization algorithm with the detailed age-specific influenza transmission model. The time-based intervention policy comprises a sequential series of actions $A_1, A_2, ..., A_T$ implemented over the time span T. The objective involves rapidly searching extensive sets of time-based actions A_i (i.e., vaccination rates implemented at each time step) to identify the most effective policy for achieving public health objectives. In this study, the transmission model returns the cumulative hospitalization incidence throughout the simulation period. To mitigate dispersed vaccination timing and uneven distribution while ensuring policy stability, we introduced a smoothness constraint on the temporal distribution of vaccination coverage, defined as the

sum of squared differences in vaccination rates between consecutive time steps. The optimization function is defined as follows:

$$\min E[\sin(A_1, A_2, \dots, A_T)] + \lambda^* \sum_{i=2, j=i-1}^T (A_i - A_j)^2$$
 (3)

where the first term represents the expectation of the stochastic simulation results returned by the transmission model, and the second term constitutes the smoothness regularization term, with $\lambda = 10^{-3}$ representing the regularization coefficient.

To solve this optimization problem, we employed a tree structure to represent all possible strategies. Each tree layer corresponds to a specific time step and contains multiple nodes. Each node connects to multiple edges leading to nodes in the subsequent layer, with each edge representing a possible action at that time step. An intervention strategy is thus mapped to a unique path within the tree structure. To strategically search the tree, we implemented the Upper Confidence Bound Applied to Trees (UCT) algorithm, which selects paths using a multi-armed bandit algorithm within each tree node (5–6). Specifically, suppose we descend the tree to reach a node n connected to k edges representing possible subsequent actions e_1 , e_2 , ..., e_k . Let $N(e_i)$ denote the number of times edge e_i has been selected, and $R(e_i)$ denote the average reward from past simulations that selected edge e_i . The rule for selecting the next edge follows:

$$\arg\max_{i} \left\{ R(e_i) + c \sqrt{\frac{\ln\left(\sum_{i} N(e_i)\right)}{N(e_i)}} \right\} \tag{4}$$

where *c* represents a constant used to balance exploitation and exploration requirements. Through this strategic path sampling approach, well-performing subtrees receive more thorough exploration than those demonstrating poor performance.

Vaccine Administration Settings

The Shenzhen CDC provided vaccination data for school-aged children and other populations in Shenzhen, covering August 2023 to May 2024. Most vaccinations were administered between October and December, achieving an overall population vaccination coverage of 11.91% and a coverage rate of 59.68% among school-aged children. Notably, free, centralized vaccination services are available exclusively to school-aged children in Shenzhen, while individuals in other age groups must voluntarily visit clinics for immunization (7). To estimate vaccination rates for other age groups, we incorporated survey data on adult vaccination willingness following the COVID-19 pandemic in 2020, along with their willingness to vaccinate elderly family members and infants. Based on monthly vaccination rates recorded by the Shenzhen CDC from 2023 to 2024 and vaccination willingness across different age groups, we decomposed the vaccination rates of other populations into age-specific rates to align with the age-group categorization used in the transmission model.

Simulated Epidemiological Impact of Vaccination Strategies on Historical Influenza Outbreaks

This study reconstructed influenza transmission patterns from 2017 to 2019 and conducted a retrospective analysis to simulate the hypothetical outcomes if vaccination strategies had been implemented during this period. The fitting results demonstrate that influenza seasons during these periods spanned approximately from December 2017 to April 2018 and from November 2018 to August 2019 (Supplementary Figure S3A). The second season lasted nearly twice as long as the first, although the peak ILI+ proxy of the first season was slightly higher, with values of 0.0357 in 2017–2018 compared to 0.0293 in 2018–2019. Under the baseline vaccination strategy, where vaccines were distributed evenly across all months, 422,293 (95% CI: 365,424–479,162) symptomatic infections and 17,583 (95% CI: 15,263–19,903) hospitalizations would be averted in 2017–2018, while 841,029 (95% CI: 748,396–933,663) symptomatic infections and 35,543 (95% CI: 31,691–39,395) hospitalizations would be averted in 2018–2019. With the same vaccine supply, the optimized strategy would vaccinate 15% and 45% of school-aged children in October and November, respectively. This strategy could potentially avert 594,234 (95% CI: 517,988–670,480) symptomatic infections and 24,743 (95% CI: 21,621–27,865) hospitalizations in 2017–2018,

and 1,111,011 (95% CI: 988,746–1,233,275) symptomatic infections and 46,918 (95% CI: 41,818–52,019) hospitalizations in 2018–2019. Supplementary Figure S3B further illustrates the differences in ILI+ proxy trends among various vaccination strategies. These results highlight the potential benefits of an optimized vaccination strategy in reducing health burdens. The findings underscore the importance of timing and targeted vaccination, particularly for school-aged children, in mitigating the impact of influenza outbreaks.

Optimized Vaccination Strategies Based on Multi-Year Weighted Evaluation

From a public health perspective, an ideal vaccination strategy must demonstrate consistent robustness across diverse epidemiological scenarios rather than merely excelling in a single year. Given that disease transmission dynamics exhibit annual variation, each year constitutes an independent search scenario, necessitating exploration of a universal optimization strategy that ensures reliable performance across historical periods. While such a strategy may not achieve optimal results in every individual year, it should deliver consistently strong overall performance, thereby establishing a foundation for sustainable, stable, and efficient public health policies. In this study, we conducted five independent optimization searches annually, compiling the results into comprehensive strategy sets. To identify a universal optimal strategy, each candidate strategy was applied across all historical years, with performance evaluated using the objective function. Consequently, the evaluation results for each year required weighting and processing to derive the final optimal strategy Vac*:

$$Vac^* = \arg\min_{Vac \in V} \sum_{y=1}^{Y} w_y H_y^{Vac}$$
 (5)

where Y represents the total number of historical time periods under consideration; V is the feasible set of all possible vaccination strategies. Each strategy $Vac \in V$ is a sequence of actions $Vac = (A1, A2, ..., A_T)$ implemented at each time step t = 1, ..., T; Vac^* denotes the optimal vaccination strategy found by the optimization; H_y^{Vac} represents the proportion of hospitalizations in year y under implementation of strategy Vac. The weight w_y for year y is introduced to adjust for epidemic severity within the objective function and can be defined as follows:

$$w_y = \frac{1}{\text{ILI} + {\text{NoVac} \over y}}$$
 (6)

where ILI+ $_{y}^{\text{NoVac}}$ represents the ILI+ proxy for year y under a no-vaccination scenario.

REFERENCES

- Yang W, Cowling BJ, Lau EHY, Shaman J. Forecasting influenza epidemics in Hong Kong. PLoS Comput Biol 2015;11(7):e1004383. https://doi.org/ 10.1371/journal.pcbi.1004383.
- 2. Doyon-Plourde P, Przepiorkowski J, Young K, Zhao LL, Sinilaite A. Intraseasonal waning immunity of seasonal influenza vaccine a systematic review and meta-analysis. Vaccine 2023;41(31):4462 71. https://doi.org/10.1016/j.vaccine.2023.06.038.
- 3. Yang W, Karspeck A, Shaman J. Comparison of filtering methods for the modeling and retrospective forecasting of influenza epidemics. PLoS Comput Biol 2014;10(4):e1003583. https://doi.org/10.1371/journal.pcbi.1003583.
- Pei S, Teng X, Lewis P, Shaman J. Optimizing respiratory virus surveillance networks using uncertainty propagation. Nat Commun 2021;12(1):222. https://doi.org/10.1038/s41467-020-20399-3.
- 5. Kocsis L, Szepesvári C. Bandit based monte-carlo planning. In: Proceedings of the 17th European conference on machine learning. Berlin, Germany: Springer. 2006; p. 282-93. http://dx.doi.org/10.1007/11871842_29.
- 6. Auer P, Cesa-Bianchi N, Fischer P. Finite-time analysis of the multiarmed bandit problem. Mach Learn 2002;47(2):235 56. https://doi.org/10.1023/A:1013689704352.
- 7. Public Hygiene and Health Commission of Shenzhen Municipality. Flu vaccines have arrived, and these people in Shenzhen will get them for free soon. 2023. https://wjw.sz.gov.cn/ztzl/ymjz/xgzc/content/post_10938913.html. [2024-7-22]. (In Chinese).
- 8. Shenzhen Municipality Bureau of Statistics. Shenzhen Statistical Yearbook 2022. 2023. https://tjj.sz.gov.cn/zwgk/zfxxgkml/tjsj/tjnj/content/post_10390917.html. [2024-5-15]. (In Chinese)
- 9. Shenzhen Municipality Bureau of Statistics. The Seventh National Population Census of Shenzhen. 2022. https://tjj.sz.gov.cn/ztzl/zt/szsdqcqgrkpc/. [2024-2-8]. (In Chinese)
- 10. Mistry D, Litvinova M, Pastore Y Piontti A, Chinazzi M, Fumanelli L, Gomes MFC, et al. Inferring high-resolution human mixing patterns for disease modeling. Nat Commun 2021;12(1):323. https://doi.org/10.1038/s41467-020-20544-y.
- 11. Du ZW, Fox SJ, Ingle T, Pignone MP, Meyers LA. Projecting the combined health care burden of seasonal influenza and COVID-19 in the 2020-2021 season. MDM Policy Pract 2022;7(1):23814683221084631. http://dx.doi.org/10.1177/23814683221084631.
- 12. Boëlle PY, Ansart S, Cori A, Valleron AJ. Transmission parameters of the A/H1N1 (2009) influenza virus pandemic: a review. Influenza Other Respir Viruses 2011;5(5):306 16. https://doi.org/10.1111/j.1750-2659.2011.00234.x.
- 13. Wu JT, Leung GM, Lipsitch M, Cooper BS, Riley S. Hedging against antiviral resistance during the next influenza pandemic using small stockpiles of

China CDC Weekly

- an alternative chemotherapy. PLoS Med 2009;6(5):e1000085. https://doi.org/10.1371/journal.pmed.1000085.
- 14. Yang Y, Sugimoto JD, Halloran ME, Basta NE, Chao DL, Matrajt L, et al. The transmissibility and control of pandemic influenza A (H1N1) virus. Science 2009;326(5953):729 33. https://doi.org/10.1126/science.1177373.
- 15. Chen DQ, Jiang YW, Huang F, Wu XL, Ye ZJ, Wu Y, et al. Effectiveness of influenza vaccination for school-age children in preventing school absenteeism in Shenzhen: an empirical study. Chin J Epidemiol 2021;42(10):1900 6. https://doi.org/10.3760/cma.j.cn112338-20210723-00580.
- Zhou YH, Tang J, Zhang JJ, Wu QS. Impact of the coronavirus disease 2019 epidemic and a free influenza vaccine strategy on the willingness of residents to receive influenza vaccines in Shanghai, China. Hum Vaccin Immunother 2021;17(7):2289 92. https://doi.org/10.1080/21645515.2020. 1871571.

Preplanned Studies

Phylogenetic and Molecular Characteristics of An H3N8 Avian Influenza Virus Detected in Wild Birds — Beijing, China, September 2024

Jiachen Zhao^{1,2,3}; Lipeng Liu⁴; Lili Li⁴; Dan Wu^{1,2,3}; Chunna Ma^{1,2,3}; Yimeng Liu^{1,2,3}; Weixian Shi^{1,2,3}; Xiaomin Peng^{1,2,3}; Shujuan Cui^{1,2,3}; Daitao Zhang^{1,2,3}; Guilan Lu^{1,2,3,#}

Summary

What is already known about this topic?

The H3N8 avian influenza virus (AIV) demonstrates considerable capacity for interspecies transmission and has been documented in multiple mammalian hosts, including equine and canine species. During 2022–2023, three laboratory-confirmed human infections with H3N8 were reported in China, heightening public health concerns about the zoonotic spillover potential of H3 subtype AIVs.

What is added by this report?

This study reports the isolation of a genetically reassorted, low-pathogenicity H3N8 avian influenza virus (AIV) from an islet in Niukouyu Wetland Park, Beijing Municipality — the first detection of this viral strain in a wild environment within the city. Throat swabs collected from park staff tested negative influenza viruses. Phylogenetic demonstrated that the viral hemagglutinin gene originated from the Eurasian lineage, while the neuraminidase gene was derived from the North American lineage. Although no direct evidence of human infection has been documented, multiple mutations identified in the virus's internal genes are associated with enhanced replication capacity, increased virulence, and improved adaptation to mammalian hosts. These molecular features indicate a potential risk for cross-species transmission to humans.

What are the implications for public health practice?

Given the potential threat that H3N8 AIVs pose to mammalian species, including humans, this study emphasizes the critical need to strengthen influenza surveillance networks and broaden monitoring efforts specifically targeting H3 subtype AIVs.

ABSTRACT

Introduction: The H3N8 avian influenza virus (AIV) is recognized for its capacity for interspecies transmission and has been detected in multiple mammalian hosts. Between 2022 and 2023, three human infections with H3N8 were documented in China, raising significant concerns about its zoonotic spillover potential. In this study, we characterized an H3N8 isolate from Niukouyu Wetland Park in Beijing Municipality to elucidate the genetic variability and evolutionary dynamics of this AIV subtype.

Methods: The virus underwent whole-genome sequencing followed by comprehensive molecular and phylogenetic characterization.

Results: We identified a genetically reassorted, lowpathogenicity H3N8 AIV, marking the first detection of this subtype in a wild environment in Beijing. Throat swabs from the park staff tested negative for influenza viruses. Phylogenetic analyses demonstrated that the viral hemagglutinin and neuraminidase genes originated from Eurasian and North American respectively. lineages, Nucleotide sequence comparisons revealed 97.57%–99.06% similarity between the eight gene segments of this virus and those of reference strains. Multiple internal gene mutations were identified, including PB2-K318R and PB1-F2-N66S, which are associated with enhanced polymerase activity, increased virulence, and improved mammalian adaptation.

Conclusions: The molecular characteristics of this H3N8 virus indicate a potential risk for cross-species transmission to humans, emphasizing the critical need to strengthen influenza surveillance networks and expand monitoring efforts targeting H3 subtype AIVs.

Avian influenza viruses (AIVs) pose a persistent

threat to poultry, mammals, and humans due to their mutation complex high rates, reassortment mechanisms, and capacity for interspecies transmission. Among all influenza A virus subtypes, those belonging to the H3Ny group demonstrate the broadest host range. Notably, the H3N8 subtype has been detected in diverse mammalian hosts, including dogs (1), donkeys (2), horses (3), pigs (4), harbor seals (5), and humans (6). To date, three laboratory-confirmed human infections with H3N8 AIV have been reported globally, all occurring in China (6-7). Given this epidemiological context, active surveillance of AIVs in regions with high spillover potential remains crucial for public health preparedness. Beijing Municipality, situated within the East Asian-Australasian Flyway, harbors wetland ecosystems that serve as critical stopover and breeding sites for migratory birds. These high-risk areas represent interfaces for reassortment and cross-species transmission. In this study, we performed whole-genome sequencing of an H3N8 virus identified from environmental surveillance samples collected in Beijing during September 2024. We conducted subsequent phylogenetic and molecular analyses to characterize the genetic evolution of this virus and identify key mutations. This investigation aimed to elucidate the genetic variability and evolutionary dynamics of H3N8 AIVs circulating in Beijing, China.

During September 2024, a total of 3,110 environmental specimens from wild birds and domestic poultry (including feces, water samples, and environmental surface swabs) were collected from 8 districts of Beijing: Daxing, Huairou, Shunyi, Miyun, Tongzhou, Fangshan, Xicheng, and Yanqing. Realtime PCR was performed using the Influenza A Virus Nucleic Acid Detection Kit (PCR-Fluorescence Probing) (Londe Medical Co., Ltd., Cat. No. V2.1) to identify influenza A virus in the collected environmental samples. A multiplex real-time PCR method was performed using the AIVs Typing Test Kit (MABSKY BIO-TECH CO., LTD., SKY-8908F) to detect the subtypes of positive samples. Following AIV identification, throat swab tests were performed on staff members from an islet in Niukouyu Wetland Park, Fangshan District.

The genome of the A/environment/Beijing/03/2024 (H3N8) (BJ03) virus was amplified using a SuperScript[®] III One Step RT-PCR Platinum Taq HiFi kit (Invitrogen, USA), and sequencing libraries were prepared using a Nextera XT DNA sample preparation kit. Whole-genome sequencing was

performed on the Illumina MiniSeq platform with a 2×150 bp paired-end sequencing kit. Raw sequencing data were processed and assembled using CLC Workbench (version 10, QIAGEN, Germany), yielding complete genome sequences for all segments with an average coverage depth exceeding 800x, thereby ensuring that 100% of genomic regions were covered by at least 100 reads. The eight gene segments of the assembled BJ03 genome were submitted to the NCBI BLAST online tool for homology comparison. For phylogenetic analysis, reference strains included 1) representative classical H3N8 strains, 2) strains exhibiting high genetic similarity to the BI03 isolate, and 3) known human-infecting H3N8 strains. Reference sequences were downloaded from the NCBI and GISAID databases for multiple sequence alignment (performed using **MEGA** 6.0) phylogenetic tree construction. Phylogenetic trees were constructed using the neighbor-joining method in 1,000 bootstrap MEGA 6.0 with replicates. Glycosylation site prediction of the BJ03 HA and NA amino acid sequences was performed using NetNGlyc (version 1.0, Lyngby, Denmark).

Analysis of collected specimens revealed AIV positivity in 43 samples: 3 for H3N8, 35 for H7N1 (all detected in Niukouyu Wetland Park in March 2024), and 3 for H5N1. Additionally, 2 specimens tested positive for mixed H5N1 and H9 AIVs. The identification of H3N8 AIV from the Niukouvu Wetland Park sample represents the first detection of this subtype in a wild environment in Beijing. One of the three H3N8-positive specimens, designated A/environment/Beijing/03/2024(H3N8) (EPI ISL 20063625) and hereafter referred to as BI03, was successfully sequenced. Following detection of H3N8 viruses in the environmental sample, staff members working on the wetland park islet underwent influenza testing. All staff members tested negative for influenza viruses and remained asymptomatic throughout the surveillance period.

BLAST analysis revealed that the *HA* and *NA* genes of BJ03 exhibited the highest nucleotide sequence similarity with the corresponding genes of A/Wild duck/South Korea/KNU2020-104/2020(H3N8) and A/Muscovy duck/Vietnam/HN5257/2019(H4N8), respectively (Table 1). The *PB2* gene demonstrated 99.06% nucleotide identity with that of an H4N6 AIV isolated from chickens in Vietnam, whereas the *PB1* gene showed the greatest similarity to that of an H7N6 AIV from wild birds in China. The *PA*, *NP*, and *M* genes of BJ03 exhibited the highest sequence similarity

TABLE 1. Nucleotide sequence similarity of BJ03 gene segments, an H3N8 AIV identified in Beijing in 2024, compared with those of other AIVs.

Gene	Length (bp)	Strain with the highest similarity	NCBI ID	Similarity (%)
PB2	2,341	A/chicken/Viet Nam/LBFecal200LC/2021(H4N6)	PV410220.1	99.06
PB1	2,297	A/wild bird/China/SUB12913325.2/2021(H7N6)	OQ509912.1	98.48
PA	2,199	A/duck/Tottori/311215/2020(H5N2)	LC656332.1	98.54
HA	1,701	A/wild duck/South Korea/KNU2020-104/2020(H3N8)	OK236003.1	98.41
NP	1,551	A/duck/Bangladesh/58751/2023(H6N2)	PP680426.1	98.64
NA	1,433	A/Muscovy duck/Vietnam/HN5257/2019(H4N8)	MW935581.1	97.56
М	982	A/duck/Akita/51019/2017(H5N3)	MK592464.1	98.78
NS	855	A/environment/Bangladesh/42635/2020(H10N7)	MW466161.1	98.60

Abbreviation: AIV=Avian Influenza Virus; PB2=Polymerase Basic 2; PB1=Polymerase Basic 1; PA=Polymerase Acidic; HA=Hemagglutinin; NP=Nucleoprotein; NA=Neuraminidase; M=Matrix; NS=Non-Structural; NCBI=National Center for Biotechnology Information.

to the corresponding genes from H5N2, H6N2, and H5N3 AIVs isolated from ducks in Tottori (Japan), Bangladesh, and Akita (Japan), respectively. The *NS* gene was most similar to that of an H10N7 AIV detected in an environmental sample from Bangladesh.

Phylogenetic analysis of the HA gene from BJ03 demonstrated that this virus belongs to the Eurasian lineage (Figure 1A). The amino acid sequence at the HA cleavage site (PEKQTR ↓ GLF) contains only one basic residue, consistent with low-pathogenicity AIV characteristics. Amino acid mutations identified in this and other genes (6,8), compared with those from reference viruses, are summarized in Table 2. The α -2,3 sialic acid receptor-binding sites of BJ03 retained the avian-origin residues Q242 and G244 without mutations (6). Additional receptor-binding motifs, including 151GSG and 206EQTN, also remained unchanged (6). Analysis of the BJ03 HA amino acid sequence identified six potential N-linked glycosylation ²⁴NSTA, ³⁸NGTI, ⁵⁴NATE, ¹⁸¹NVTM, sites: ³⁰¹NGSI, and ⁴⁹⁹NGTY. All six sites exhibited high conservation when compared with those of the reference strains.

The full-length *NA* gene of BJ03 spans 1,433 bp, encoding 476 amino acids, and phylogenetically clusters within the North American lineage (Figure 1B). Examination of antiviral resistance sites revealed an I312V substitution, suggesting potential alterations in oseltamivir susceptibility. Furthermore, four putative N-linked glycosylation sites were identified within the *NA* sequence: ⁴⁶NETV, ⁵⁴NETV, ¹⁴⁴NGTV, and ²⁹³NWTG.

Analysis of the internal genes of BJ03 revealed multiple key mutations: K318R, K389R, and V598T in *PB2*; L13P and L473V in *PB1*; N66S in *PB1-F2*; K26E and V160D in *PA*; K398Q in *NP*; N30D and

T215A in *M1*; V27I in *M2*; and P42S in *NS1* (Table 2). These mutations are associated with enhanced virulence, pathogenicity, and mammalian host adaptation.

DISCUSSION

The H3 and N8 genes of BJ03 exhibited high nucleotide similarity with H3 subtypes circulating in wild ducks in Korea and N8 subtypes prevalent in Muscovy ducks in Vietnam, respectively. The internal genes demonstrated high nucleotide similarity with those of low-pathogenicity avian influenza virus (LPAIV) subtypes H4, H5, H6, H7, and H10 previously identified in northeastern China, Vietnam, Japan, and Bangladesh. These findings suggest that BJ03 represents a reassortant virus generated through co-infection of a single avian host by multiple AIV subtypes along migratory flyways. Genetic exchange and reassortment among different LPAIV subtypes occur frequently in nature and can generate novel highly pathogenic strains when highly pathogenic AIVs reassortment within the host Consequently, LPAIVs not only carry an intrinsic risk of genetic evolution but also pose a substantial threat to public health.

The Eurasian lineage of the *H3* gene and North American lineage of the *N8* gene in BJ03 are consistent with patterns observed in human-infecting H3N8 AIV strains, including A/Changsha/1000/2022(H3N8), A/Henan/4-10CNIC/2022(H3N8), and A/Guangdong/ZS-2023SF005/2023(H3N8). Studies in southern China have demonstrated that reassortment between Eurasian and North American lineage genes is common among H3Ny subtypes (*10*). Migratory birds can harbor viruses carrying this *N8*

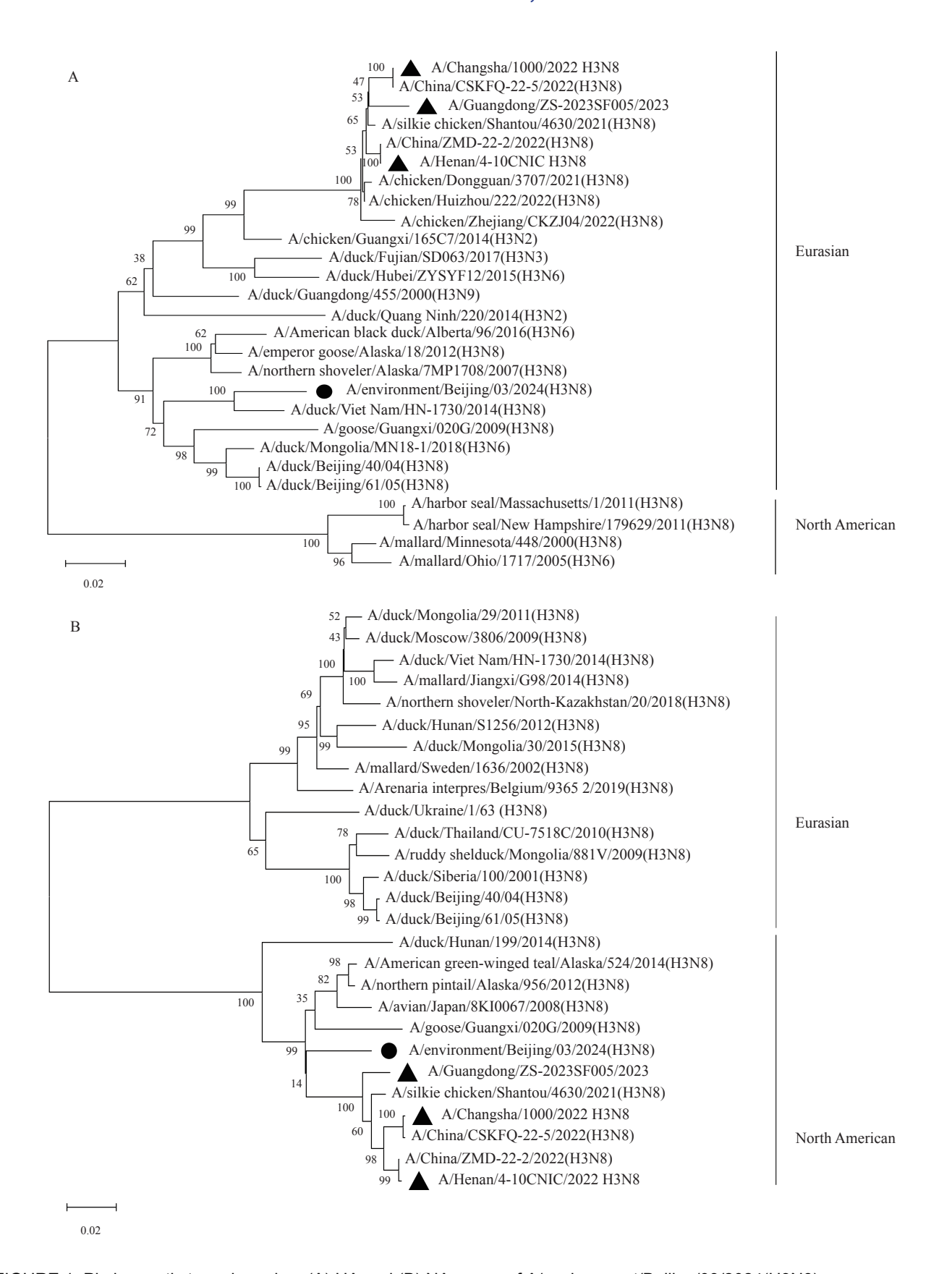


FIGURE 1. Phylogenetic trees based on (A) HA and (B) NA genes of A/environment/Beijing/03/2024(H3N8). Note: ● means BJ03 specimen from this study; ▲ means reference H3N8 avian influenza virus strains previously associated with human infections.

Abbreviation: HA=hemagglutinin; NA=neuraminidase.

TABLE 2. Comparison of key sites in the predicted amino acid sequences encoded by the genes of BJ03 (an H3N8 AIV identified in Beijing in 2024) with those of other isolates.

Gene '	Amino acid	Phenotypic characteristics	Isolate					
Gene	sites	Filehotypic characteristics	BJ03	AHTT41	HK110MA213	GD01	BJ40	GX020G
	¹⁵¹ GSG ¹⁵³	Receptor binding site	GSG	GSS	GSN	GSG	GSN	QSA
	²⁰⁶ EQTN ²⁰⁹	Receptor binding site	EQTN	EQTN	EQTS	EQTN	EQTN	EQTN
HA	Q242L	Receptor binding site	Q	Q	L	Q	Q	Q
	G244S	Receptor binding site	G	G	S	G	G	G
	Cleavage sites	3	PEKQTF ↓GLF	RPEKQTR ↓GLF	PEKQTR ↓GLF	PEKQTF	PEKQTF ↓GLF	RPEKQTR ↓GLF
NA	I312V	Increased resistance to oseltamivir	V	S	V	V	V	V
	1292V	Mammalian host adaptation	1	1	Т	V	1	1
	K318R	Mammalian host adaptation	R	R	R	R	R	R
PB2	K389R	Increased virus replication ability in mammals	R	R	R	K	R	R
FD2	V598T	Increased virus replication ability in mammals	Т	Т	Т	V	Т	Т
	E627K	Mammalian host adaptation	E	E	K	Е	E	E
	D701N	Mammalian host adaptation	D	D	D	D	D	D
PB1	L13P	Mammalian host adaptation	Р	Р	Р	Р	Р	Р
PDI	L473V	Mammalian host adaptation	V	V	V	V	V	V
PB1-F2	N66S	Increased virulence in mice	S	N	N	N	S	N
	K26E	Mammalian host adaptation	E	E	E	Е	Е	E
PA	V160D	Mammalian host adaptation	D	D	D	D	D	D
	K356R	Mammalian host adaptation	K	K	R	R	K	K
NP	K398Q	Mammalian host adaptation	Q	Q	Q	Q	Q	Q
	V15I	Mammalian host adaptation	V	V	V	I	V	V
M1	N30D	Increase pathogenicity and transmission in mammals	s D	D	D	D	D	D
	T215A	Increased virulence in mammals	Α	Α	Α	Α	Α	Α
М2	V27A/I/T	Increased resistance to adamantane	I	V	V	V	V	V
IVI∠	S31N	Increased resistance to adamantane	S	S	S	Ν	S	s
NS1	P42S	Increased virulence in mice	S	S	S	S	Α	S

Note: BJ03 refers to specimen A/environment/Beijing/03/2024(H3N8), AHTT41 to reference strain A/Anseriformes/Anhui/TT41/2014(H3N8), HK110MA213 to reference strain A/Hong Kong/1-10-MA21-3/1968(H3N2), GD01 to reference strain A/chicken/China/Guangdong/01/2022(H3N8), BJ04 to reference strain A/duck/Beijing/40/04(H3N8), and GX020G to reference strain A/goose/Guangxi/020G/2009(H3N8). Abbreviation: AIV=Avian Influenza Virus; PB2=Polymerase Basic 2; PB1=Polymerase Basic 1; PA=Polymerase Acidic; HA=Hemagglutinin; NP=Nucleoprotein: NA=Neuraminidase; M=Matrix; NS=Non-Structural.

gene for extended periods, introducing them into domestic regions along the East Asia–Australasia flyway (11). This flyway represents a major migratory corridor connecting the Arctic Circle to Australia and hosts the greatest diversity and abundance of migratory bird species among the world's nine major flyways. The route spans a coastal wetland network stretching from the Russian Far East to Australia, encompassing 22 countries and regions. Given Beijing's location along this flyway, similar reassortment events may occur in this region. However, further surveillance studies are required to confirm this hypothesis.

Although BJ03 shares the same "Eurasian H3–North

American N8" genomic framework with human-infecting H3N8 strains, its H3 gene is phylogenetically distant from those strains, whereas its N8 gene exhibits closer phylogenetic relatedness. This pattern highlights the complex ecological and evolutionary dynamics underlying H3N8 virus distribution. In China, H3 subtypes demonstrate a clear pattern of multiple co-circulating sublineages (12). The concurrent detection of H3N8 and H7N1 viruses in Niukouyu Wetland Park exemplifies the broader co-circulation pattern of multiple AIV subgroups and lineages observed throughout China. Although these sublineages share genetic homology, they have diverged through

geographical isolation and host adaptation. The regional coexistence of distinct subgroup viruses, such as H3N8 and H7N1, increases the probability of genetic reassortment due to overlapping host ranges — both subtypes readily infect ducks and other waterfowl. The N8 gene, which originated in North America and was introduced into Eurasia relatively recently by migratory birds, appears to have been maintained through avian transmission with minimal genetic variation. Nevertheless, the prolonged coexistence of this N8 gene with the locally prevalent H3 gene and other circulating subgroup viruses (such as H7N1) creates ongoing opportunities for adaptive mutation accumulation and genetic reassortment events.

The surface-expressed hemagglutinin (HA) glycoprotein plays a pivotal role in determining AIV pathogenicity and virulence, with its cleavage site sequence serving as a critical molecular marker. In predicted cleavage site PEKQTR

GLF contains a single basic amino acid residue, which is consistent with the molecular characteristics of HAs from LPAIVs. Residues O242 and G244 on the HA protein represent canonical amino acids of avian origin and indicate a preferential binding affinity for avian-type receptors. Although glycosylation sites on the HA protein, particularly those near the receptor-binding domain, may influence viral virulence (13-15), no such glycosylation sites were identified near the receptor-binding domain in BI03 (13). Nonetheless, the predicted proteins of BI03 harbor several mutations associated with increased virulence in mammalian hosts, including N66S in PB1-F2, T215A and N30D in M1, and P42S in NS1 (14–16). These mutations have been linked to enhanced virulence in mice and increased pathogenicity and transmissibility in (14–16). Additionally, several mammalian-adaptive mutations were detected, including K318R, K389R, and V598T in PB2; L13P and L473V in PB1; K26E and V160D in PA; and K398Q in NP (17). The presence of these mutations suggests that the BJ03 virus possesses considerable potential to cross the species barrier and infect humans, warranting heightened surveillance of H3 subtype AIVs. Furthermore, the mutations I312V in N8 and V27I in M2 suggest possible increased resistance to oseltamivir and amantadine, respectively; however, these findings require further experimental validation.

Although this study did not identify direct evidence of human infection with H3N8 AIVs, the molecular features of BJ03 suggesting mammalian host

adaptation underscore a potential risk for zoonotic transmission. To date, all confirmed human infections with H3N8 AIVs have occurred in China, including two pediatric cases in 2022 and one adult female case in 2023 — the latter representing the first fatal H3N8 infection reported globally (6,18). All three cases involved prior exposure to live poultry, and in two instances, wild birds were reportedly active near the residences. Although human-to-human patients' transmission has not been documented, the propensity for genetic reassortment and the complexity of internal genes in H3N8 AIVs raise significant concerns regarding their pandemic potential (19). Consequently, sustained surveillance for pandemic risk remains critical. We recommend implementing a reinforced surveillance strategy that includes: 1) enhancing monitoring and information feedback systems in key areas with high wild bird activity; 2) establishing robust surveillance networks to ensure timely detection and reporting; and 3) strengthening multi-sectoral collaboration across public health, veterinary, and wildlife management agencies. A notable limitation of this study is the absence of in vitro or in vivo pathogenicity assessments. While our phylogenetic and molecular analyses provide compelling genetic evidence for the virus's potential mammalian adaptation and associated risks, these findings require functional validation through future experimental studies.

In conclusion, the H3N8 virus identified in this study exhibits genetic characteristics indicative of potential cross-species transmission to humans. Continuous surveillance and comprehensive risk assessment remain essential to mitigate the threat of emerging public health emergencies posed by avian influenza viruses.

Conflicts of interest: No conflicts of interest.

Funding: Beijing Natural Science Foundation - Haidian Original Innovation Joint Fund (No.L232073) and Highlevel Public Health Technical Talent Construction Project (Key member-02-11).

doi: 10.46234/ccdcw2025.233

Copyright © 2025 by Chinese Center for Disease Control and Prevention. All content is distributed under a Creative Commons Attribution Non Commercial License 4.0 (CC BY-NC).

^{*} Corresponding author: Guilan Lu, luguilan@bjcdc.org.

¹ Beijing Center for Disease Prevention and Control, Beijing, China;
² Beijing Key Laboratory of Surveillance, Early Warning and Pathogen Research on Emerging Infectious Diseases Beijing Research Center for Respiratory Infectious Diseases, Beijing, China;
³ Beijing Research Center for Respiratory Infectious Diseases, Beijing, China;
⁴ Fangshan District Center for Disease Control and Prevention, Beijing, China.

Submitted: August 25, 2025 Accepted: October 25, 2025 Issued: October 31, 2025

REFERENCES

- Martinez-Sobrido L, Blanco-Lobo P, Rodriguez L, Fitzgerald T, Zhang HY, Nguyen P, et al. Characterizing emerging canine H3 influenza viruses. PLoS Pathog 2020;16(4):e1008409. https://doi.org/10.1371/ journal.ppat.1008409.
- Qi T, Guo W, Huang WQ, Dai LL, Zhao LP, Li HM, et al. Isolation and genetic characterization of H3N8 equine influenza virus from donkeys in China. Vet Microbiol 2010;144(3-4):455 – 60. https://doi. org/10.1016/j.vetmic.2010.01.006.
- Miño S, Mojsiejczuk L, Guo W, Zhang HL, Qi T, Du C, et al. Equine influenza virus in Asia: phylogeographic pattern and molecular features reveal circulation of an autochthonous lineage. J Virol 2019;93(13): e00116 – 19. https://doi.org/10.1128/JVI.00116-19.
- Tu JG, Zhou HB, Jiang TZ, Li C, Zhang AD, Guo XB, et al. Isolation and molecular characterization of equine H3N8 influenza viruses from pigs in China. Arch Virol 2009;154(5):887 – 90. https://doi.org/10. 1007/s00705-009-0381-1.
- Karlsson EA, Ip HS, Hall JS, Yoon SW, Johnson J, Beck MA, et al. Respiratory transmission of an avian H3N8 influenza virus isolated from a harbour seal. Nat Commun 2014;5:4791. https://doi.org/10. 1038/ncomms5791.
- Yang RG, Sun HL, Gao F, Luo KW, Huang Z, Tong Q, et al. Human infection of avian influenza A H3N8 virus and the viral origins: a descriptive study. Lancet Microbe 2022;3(11):e824 – 34. https://doi. org/10.1016/S2666-5247(22)00192-6.
- Feng XQ, Li LM, Wang J, Wu GS, Li Y. One case of severe pneumonia and death from H3N8 influenza in human. Chin J Lab Med 2023;46 (9):950 – 4. https://doi.org/10.3760/cma.j.cn114452-20230423-00209.
- 8. Zhang H, Han SY, Wang B, Xing YN, Yuan GH, Wang Y, et al. Genetic characterization and pathogenesis of avian influenza virus H3N8 isolated from *Chinese pond heron* in China in 2021. Viruses 2023;15(2):383. https://doi.org/10.3390/v15020383.
- 9. Wang JL, Li XY, Fan J, Guo J, Deng GH, Shi JZ, et al. Sequence

- analysis and pathogenesis of H9N2 avian influenza viruses in mice. Chin J Prev Vet Med 2013;35(8):663 5. https://doi.org/10.3969/j. issn.1008-0589.2013.08.15.
- Yang JY, Yang L, Zhu WF, Wang DY, Shu YL. Epidemiological and genetic characteristics of the H3 subtype avian influenza viruses in China. China CDC Wkly 2021;3(44):929 – 36. https://doi.org/10. 46234/ccdcw2021.225.
- Olsen B, Munster VJ, Wallensten A, Waldenström J, Osterhaus ADME, Fouchier RAM. Global patterns of influenza A virus in wild birds. Science 2006;312(5772):384 – 8. https://doi.org/10.1126/ science.1122438.
- 12. Yang JY, Zhang Y, Yang L, Li XY, Bo H, Liu J, et al. Evolution of avian influenza virus (H3) with spillover into humans, China. Emerg Infect Dis 2023;29(6):1191 201. https://doi.org/10.3201/eid2906.221786.
- Perdue ML, Latimer J, Greene C, Holt P. Consistent occurrence of hemagglutinin variants among avian influenza virus isolates of the H7 subtype. Virus Res 1994;34(1):15 – 29. https://doi.org/10.1016/0168-1702(94)90116-3.
- 14. Fan SF, Deng GH, Song JS, Tian GB, Suo YB, Jiang YP, et al. Two amino acid residues in the matrix protein M1 contribute to the virulence difference of H5N1 avian influenza viruses in mice. Virology 2009;384(1):28 32. https://doi.org/10.1016/j.virol.2008.11.044.
- Sun YP, Hu Z, Zhang XX, Chen MY, Wang Z, Xu GL, et al. An R195K mutation in the PA-X protein increases the virulence and transmission of influenza A virus in mammalian hosts. J Virol 2020;94 (11):e01817 – 19. https://doi.org/10.1128/JVI.01817-19.
- Mei K, Liu G, Chen ZZ, Gao ZM, Zhao LH, Jin T, et al. Deep sequencing reveals the viral adaptation process of environment-derived H10N8 in mice. Infect Genet Evol 2016;37:8 – 13. https://doi.org/10. 1016/j.meegid.2015.10.016.
- Carnaccini S, Perez DR. H9 influenza viruses: an emerging challenge. Cold Spring Harb Perspect Med 2020;10(6):a038588. https://doi.org/ 10.1101/cshperspect.a038588.
- Zhuang YL, Wang M, Liang LJ, Mao YX, Wang KB, Yang SH, et al. First known human death after infection with the avian influenza A/ H3N8 virus: Guangdong Province, China, March 2023. Clin Infect Dis 2024;78(3):646 – 50. https://doi.org/10.1093/cid/ciad462.
- Shen Y, Liu YH, Krafft T, Wang QY. Progress and challenges in infectious disease surveillance and early warning. Med Plus 2025;2(1): 100071. https://doi.org/10.1016/j.medp.2025.100071.

Methods and Applications

Developing Machine Learning Prediction Model for Daily Influenza Reported Cases Using Multichannel Surveillance Data — A City, Hubei Province, China, 2023–2025

Xinyue Zhang¹; Xinyi Sang¹; Beibei Liu¹; Quanyu Wang¹; Xiuran Zuo²; Sheng Wei^{1,3,#}; Qi Wang^{1,#}

ABSTRACT

Introduction: Public health surveillance is crucial for decision-making. Given the significant threat of influenza to public health, developing predictive models using multichannel surveillance systems is imperative.

Methods: Data were collected from multichannel surveillance systems, including hospitals, search engines, and climatological and air pollutant surveillance systems, in a southern Chinese city from January 2023 to January 2025. Spearman's correlation analysis assessed the relationships between variables and reported influenza cases. Several machine learning models were used to predict trends in reported cases.

Results: Correlation analysis showed that all four surveillance systems were related to influenza, with 27 variables correlated with daily reported cases. The Long Short-Term Memory model, established based on variables with the highest lagged correlations (5-day to 7-day lag) through combined surveillance systems, outperformed other models for 5-day forecasts (R²=0.92; mean absolute error=156.92; mean absolute percentage error=79.95%; root Mean Squared Error=292.33).

Conclusions: Data from various surveillance systems effectively track influenza epidemics. The model shows potential for infectious disease surveillance and epidemic preparedness.

Influenza, an acute respiratory infectious disease caused by the influenza virus, threatens global public health due to its high incidence, transmissibility, and severe complications (1). Effective surveillance is crucial for timely public health interventions.

Influenza spread is influenced by climatic, human migration, social media, and socioeconomic status (2). Integrating multisource data outbreak prediction

remains challenging.

Artificial intelligence (AI) has introduced new scope in disease prediction. Deep learning (DL), a machine learning (ML) subset, enables model optimization through self-supervised learning, showing superior prediction performance (3). These technologies show potential for disease prediction by capturing complex patterns (4).

This study explored the relationship between influenza cases and surveillance systems in a southern Chinese city, using AI techniques to establish prediction models for influenza epidemics, to refine monitoring strategies and inform public health responses.

METHODS

This study was conducted in a major southern Chinese city with 13 million residents in late 2023. Located at 114° 30′ E and 30° 58′ N, it has a subtropical monsoon humid climate with hot summers and cold winters. Influenza occurs more in winter and spring. Several hospitals serve as influenza surveillance sentinel to collect representative data systematically. To build the prediction model, data were collected from multichannel surveillance systems, including influenza cases, hospitals, meteorological and air pollutant surveillance systems, and search engine data (Supplementary Table S1, available at https://weekly.chinacdc.cn/).

Multi-Surveillance systems

Daily influenza reported cases were obtained from China Information System for Disease Control and Prevention (5). All case details were identified. After tallying daily case counts, missing data for 70 days (70/731, 9%) was identified. Linear interpolation was chosen for its ability to preserve temporal structure and provide reliable estimates for short-term missing values, making it preferable to mean imputation or deletion.

Daily fever clinic attendance and nine related symptoms, including runny nose, cough, sore throat, dyspnea, fever, headache, joint pain, myalgia, and fatigue, were collected from Electronic Medical Records (EMRs) of outpatient visits.

Baidu, a Chinese search engine, provides a search index for tracking keyword trends and user behavior. Baidu Search Index (BSI) data covering desktop and mobile queries were collected using influenza symptoms keywords (https://index.baidu.com/ [accessed 2025-01-05]).

Air pollutant surveillance data, including concentrations of particulate matter with aerodynamic diameter \leq 2.5 µm (PM_{2.5}), particulate matter with aerodynamic diameter \leq 10.0 µm (PM₁₀), nitrogen dioxides (NO₂), sulfur dioxide (SO₂), carbon monoxide (CO), and ozone (O₃), were obtained from the city's Department of Ecology and Environment website.

Meteorological surveillance data were obtained from China Meteorological Data Sharing Service Center (http://data.cma.cn/en [accessed 2025-01-05]), including daily mean temperature (Tmean), mean relative humidity (RHmean), mean air pressure, mean wind speed, mean precipitation, and mean visibility range. The mean absolute humidity (AHmean) was calculated based on Tmean and RHmean as following formula (6):

```
AHmean = \{6.112 \times exp[(17.67 \times Tmean) / (Tmean \pm 243.5)] \times RHmean \times 2.1674\}/
(273.15 + Tmean)
```

Model Construction

Spearman's correlation coefficients were calculated for all variables for daily reported cases, as data showed strong non-parametric distributions. Each variable was normalized to 0–1 to facilitate model compatibility.

This study used ML methods to build prediction models: ensemble models (Random Forest and eXtreme Gradient Boosting), linear regression, and instance-based models (K-Nearest Neighbor). Two DL models, the Gated Recurrent Unit and Long Short-Term Memory (LSTM), were used.

In the model construction process, variables with P<0.05 in correlation analysis were selected as model inputs. Lagged correlations evaluated relationships between each variable and reported cases from -7 to 0 days. For prediction on day t, variables with highest correlation coefficients from t–7 to t were selected.

For the DL models, grid search determined optimal

hyperparameter combinations. The selected hidden sizes were 32, 64, 128, and 256. The number of layers ranged from one to three in steps by one. Dropout values ranged from 0.3 to 0.5 step by 0.05. The learning rate values selected were 0.01, 0.05, 0.001, and 0.0005. Adam was selected as the optimizer.

The data from January 2023 to January 2025 showed two peaks in influenza cases and an upward trend in late 2024 (Supplementary Figure S1, available at https://weekly.chinacdc.cn/). The dataset was split in an 8:2 ratio into a training set (January 2023 to August 2024) and testing set (August 2024 to January 2025) for model training and validation. This ensured adequate training data while maintaining a predictive baseline for validation. The model performance was evaluated by comparing predicted and actual data using the coefficient of determination (R²) (values close to 1 indicate better prediction), mean absolute error (MAPE), and root mean square error (RMSE) (values close to 0 indicate better prediction).

Model Comparison

To evaluate model validity and robustness of the selected dataset and constructed model, comparative analysis of the performances of the various models was conducted. Prediction models were developed using four surveillance systems: hospital (H), search engine (B), meteorological (M), and air pollutant (P). These models involved individual systems and their combinations: *Model H*, *Model B*, *Model M*, *Model P*, *Model H+B*, *Model H+M*, *Model H+P*, *Model B+M*, *Model B+P*, *Model H+M+P*, *Model B+M+P*, *Model All*, totaling 15 models.

Statistical Analysis

All the time-series data were smoothed. All statistical analyses in this study were performed using Python (version 3.12.0; Python Software Foundation, Wilmington, Delaware, USA) and TensorFlow (version 2.0.0; Google LLC, Mountain View, California, USA).

RESULTS

Description of Data from Surveillance Systems

From January 2023 to January 2025, the reported

influenza cases showed three distinct peaks (Supplementary Figure S1): the first in early 2023, second from December 2023 to January 2024, and third in late 2024. These peaks highlight the seasonal and fluctuating nature of influenza infections.

During monitoring, the number of fever clinic visits and nine symptoms showed trends similar to those of influenza cases but with discrepancies. Fever clinic visits increased in early 2023 and from October 2023 to January 2024, matching the first two peaks, but not the third in late 2024 (Supplementary Figure S2, available at https://weekly.chinacdc.cn/). The daily frequencies of nine influenza-related symptoms showed similar patterns (Supplementary Figure S3, available athttps://weekly.chinacdc.cn/). Daily BSI trends, climatic factors, and air pollutants are detailed inSupplementary Figures S4–S6 (available at https://weekly.chinacdc.cn/).

Correlation of Surveillance Systems

Figure 1 shows the lag correlations between all surveillance data and the reported cases over the monitoring period. Most correlations were statistically significant (*P*<0.001). Symptoms like sore throat, cough, and myalgia showed strong positive correlations at shorter lags (0–3 days). Myalgia reached a correlation of 0.694 [95% confidence interval (*CI*): 0.654, 0.730] at Coef-0, sore throat was 0.634 (95% *CI*: 0.588, 0.675) at Coef-0, and cough was 0.566 (95% *CI*: 0.514, 0.613) at Coef-1. The meteorological factors and air pollutants were weakly correlated. Tmean had a correlation of –0.456 at Coef-7 and –0.425 at Coef-3, while O₃ had –0.337 at Coef-7 and –0.321 at Coef-5.

Prediction Model of the Influenza Cases

Prediction models for reported influenza cases were

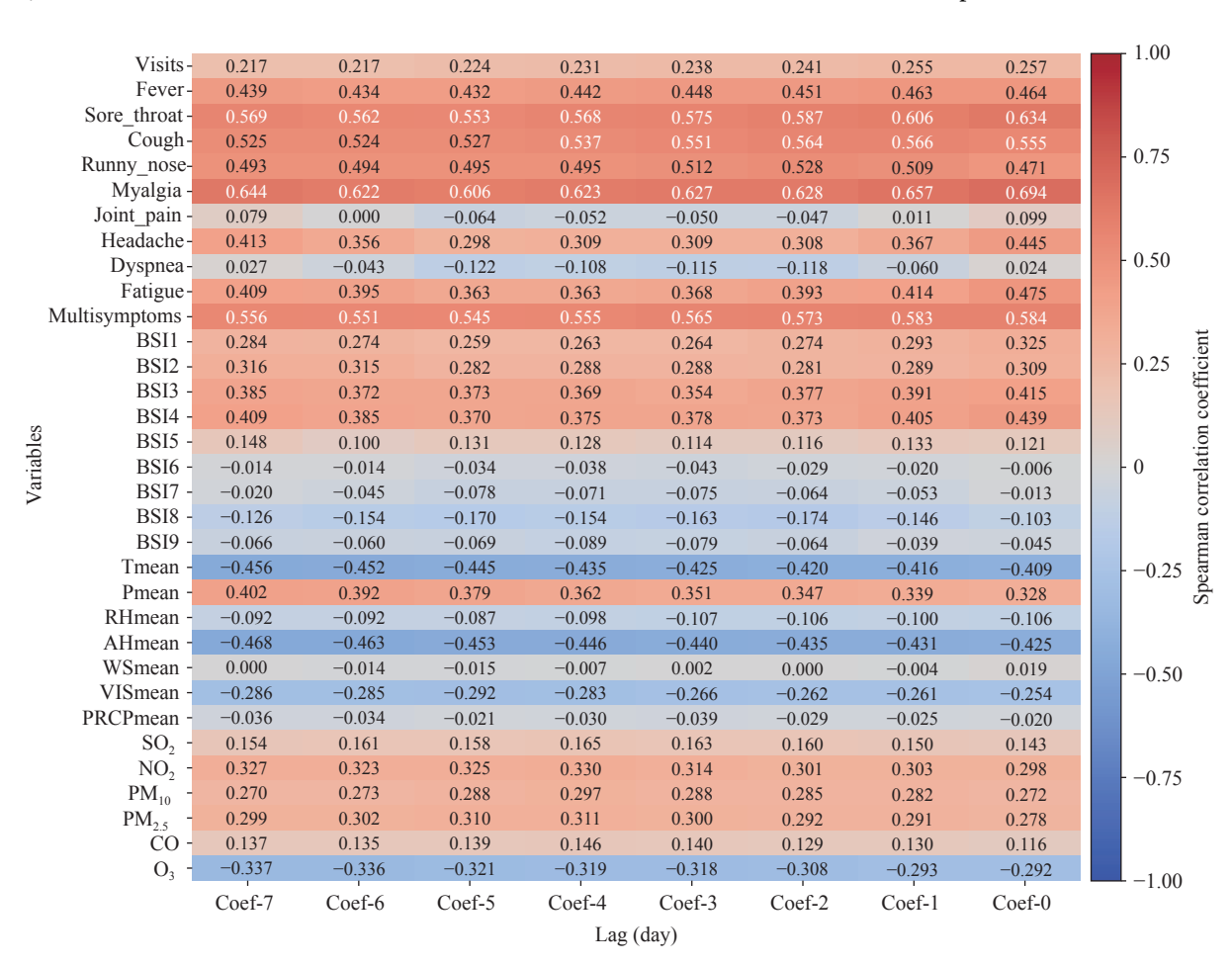


FIGURE 1. Spearman correlation analysis between different surveillance systems and reported cases with a 7-day lag before.

Abbreviation: Tmean=daily mean temperature; Pmean=daily mean air pressure; RHmean=daily mean relative humidity; AHmean=daily mean absolute humidity; WSmean=daily mean wind speed; VISmean=daily mean visibility; PRCPmean=daily mean precipitation.

developed using variables from four surveillance systems. For DL models, a temporal window was incorporated, and the LSTM model performed best with a 14-day window (R^2 =0.81, MAE=170.59, MAPE=60.26%, and RMSE=453.23) (Supplementary Table S2, available at https://weekly.chinacdc.cn/). Prediction models were then built using various ML algorithms for predictions from 0 to 7 days ahead. The LSTM model, using variables with highest lagged correlations (5- to 7-day lag), showed strong prediction performance for 5 davs forecasts $(R^2=0.92;$ MAE=156.92; MAPE=79.95%; RMSE=292.33)

(Table 1).

The prediction performances of different surveillance systems combinations were compared. The model using all variables performed the best (R²=0.92, MAE=156.92, MAPE=79.95%, and RMSE=292.33) (Figure 2). The models based on a single surveillance system performed poorly, and the best-performing model was *Model H* (R²=0.25, MAE=428.57, MAPE=221.61%, and RMSE=896.41). Among the two system combinations, *Model H+M* was best (R²=0.73, MAE=248.17, MAPE=125.64%, RMSE=533.21). For the three-system combinations, *Model*

TABLE 1. Comparison of different lag days of data between different models.

Model performance	Lag (day)							
	-7	-6	-5	-4	-3	-2	-1	0
MAE								
RF	337.87	338.28	341.30	334.08	312.13	300.46	288.00	242.29
XGBoost	287.21	278.68	306.39	296.40	256.80	270.32	262.13	194.60
LR	331.20	345.66	363.05	459.53	463.15	453.79	518.47	520.87
KNN	318.65	322.00	335.00	315.57	310.96	292.79	272.76	249.22
GRU	213.40	201.27	245.67	248.84	222.84	209.87	245.61	235.47
LSTM	200.40	229.21	156.92	238.00	244.77	258.08	214.40	170.59
MAPE (%)								
RF	123.67	126.36	133.84	134.04	129.53	127.40	124.04	118.06
XGBoost	123.83	113.94	126.43	129.99	106.45	117.50	100.04	91.91
LR	290.16	299.56	290.85	405.42	409.27	396.86	466.83	553.25
KNN	101.26	110.71	112.25	101.42	104.63	95.35	85.36	89.93
GRU	92.66	80.78	99.19	70.50	74.83	73.84	104.70	87.31
LSTM	82.45	114.17	79.95	124.37	132.32	110.60	61.55	60.26
RMSE								
RF	850.54	847.87	839.32	801.37	734.83	702.84	662.17	522.37
XGBoost	676.90	666.64	740.27	670.44	622.87	619.18	627.01	436.74
LR	563.26	575.52	607.19	665.98	659.59	653.02	699.16	601.48
KNN	835.86	824.83	840.50	789.46	792.10	753.85	721.15	572.74
GRU	416.80	505.86	611.00	646.34	553.33	509.26	574.51	581.57
LSTM	467.92	407.89	292.33	405.50	490.79	574.22	570.83	453.23
R^2								
RF	0.25	0.26	0.27	0.34	0.44	0.49	0.55	0.72
XGBoost	0.53	0.54	0.44	0.54	0.60	0.61	0.60	0.80
LR	0.67	0.66	0.62	0.54	0.55	0.56	0.50	0.63
KNN	0.28	0.30	0.27	0.36	0.35	0.41	0.46	0.66
GRU	0.84	0.76	0.65	0.61	0.71	0.76	0.69	0.68
LSTM	0.79	0.83	0.92	0.84	0.77	0.69	0.69	0.81

Abbreviation: MAE=mean absolute error; RF=Random Forest; XGBoost=eXtreme Gradient Boosting; SVM=Support Vector Machine; LR=Linear Regression; KNN=K-Nearest Neighbors; GRU=Gated Recurrent Unit; LSTM=Long Short-Term Memory; MAPE=mean absolute percentage error; RMSE=root mean square error; R²=coefficient of determination.

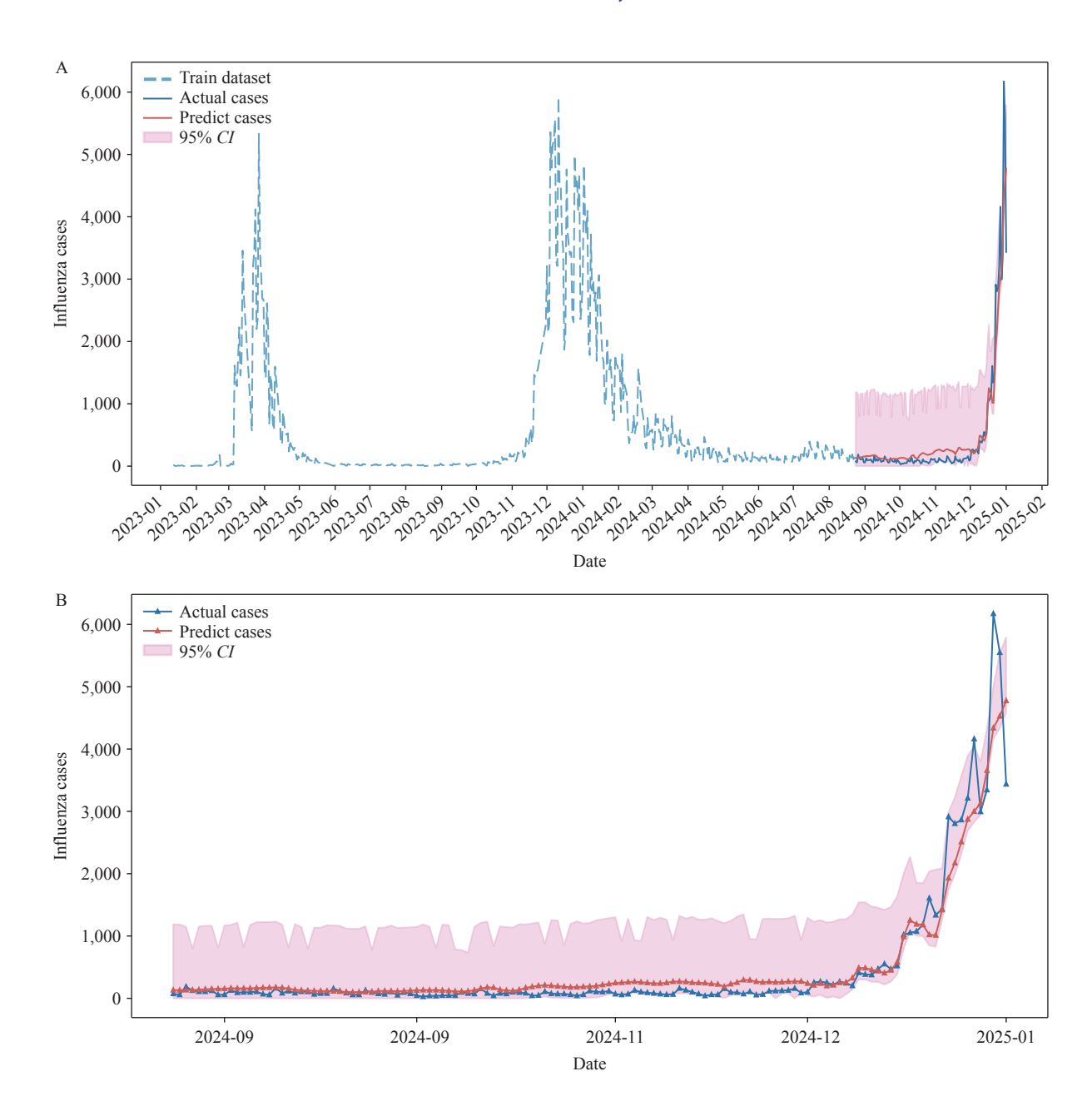


FIGURE 2. Prediction diagram for the LSTM model. (A) All monitoring period; (B) Test set period. Abbreviation: LSTM=Long Short-Term Memory; *Cl*=confidence interval.

H+M+P (R²=0.84, MAE=201.06, MAPE=63.64%, RMSE=418.51) showed the highest prediction efficiency (Table 2).

DISCUSSION

Prediction models were developed to track the influenza epidemic in a southern Chinese city by integrating data from multichannel surveillance systems. The LSTM model combining all surveillance data demonstrated high prediction accuracy, with R²=0.92, MAE=156.92, MAPE=79.95%, and RMSE=

292.33, outperforming other models.

Compared to existing models, our approach shows improved prediction accuracy by integrating multiple data sources. Previous studies relied mainly on single-source data, such as clinical report (7) or Google Trends (8), limited by reporting delays, definition changes, and data errors (9–10). Our models used EMRs, social media, meteorological, and air pollutant data were designed to mitigate forecasting errors. The combined model performed best, highlighting the value of diverse data in assessing influenza trends. The early phase of the influenza outbreak highlighted the

TABLE 2. Comparison of different combinations of data.

Model performance of different combinations	MAE	MAPE (%)	RMSE	R ²
Model H	428.57	221.61	896.41	0.25
Model B	414.27	141.49	971.23	0.11
Model M	456.34	159.50	946.81	0.16
Model P	435.46	131.86	1000.15	0.06
Model H+B	370.35	168.43	793.79	0.41
Model H+M	248.17	125.64	533.21	0.73
Model H+P	286.82	105.25	670.63	0.58
Model B+M	275.89	102.85	651.88	0.60
Model B+P	317.25	109.17	703.38	0.54
Model M+P	254.46	102.41	548.00	0.72
Model H+B+M	215.49	108.40	480.24	0.78
Model H+B+P	197.02	52.24	522.32	0.74
Model H+M+P	201.06	63.64	418.51	0.84
Model B+M+P	267.35	118.07	550.24	0.72
Model All	156.92	79.95	292.33	0.92

Abbreviation: MAE=mean absolute error; MAPE=mean absolute percentage error; RMSE=root mean square error; R²=coefficient of determination.

inadequacy of confirmed case data for traditional surveillance (11). A multifaceted monitoring approach is essential to improve epidemic predictions.

Data quality and diversity significantly affect model provide performance. **EMRs** detailed clinical information. Fever clinic visits exhibited a weaker correlation (r=0.257), as fever clinic patients may have other diseases and some patient with influenza may not visit fever clinics. Symptoms like myalgia, cough, and sore throat showed stronger positive correlations with influenza cases at shorter lags, which underscore the importance of symptom-based surveillance (12). Social media data provide real-time insights into potential outbreaks, with search volumes for symptom keywords correlating with influenza cases (13). Studies indicate that combining Internet-based queries and climate data improves the accuracy and timeliness of infectious disease warning systems (14). Our findings show positive correlations between air pollutants (SO₂, NO₂, PM₁₀, PM₂₅, and CO) and negative correlation between O3 and influenza cases, consistent with previous studies (15–16). This highlights importance of integrating air pollutant data for accurate influenza forecasting.

The LSTM model demonstrated improved accuracy through multisource data. Hospital surveillance enhanced prediction performance, consistent with correlation results. This approach provides understanding of environmental factors, public health

interventions, and disease dynamics. Although a 5–7-day lag generally performed well, some combinations weakened due to flu's complex spread mechanisms involving virus survival and human behavior. Environmental variables can extend virus survival time, potentially causing delays between changes and observable influenza case increases. Our multisource surveillance data integrated clinical, laboratory, and syndromic monitoring systems, with reporting delays contributing to extended lag period. Despite similarities in respiratory disease spread factors, significant heterogeneity existed. Early prediction improves response strategies, resource allocation, and outbreak management.

This study has certain limitations. The absence of population mobility and vaccination rates may restrict the capacity of the model to capture influenza transmission dynamics. Data quality from less reliable sources may affect performance, and the lack of external validation limits generalizability. Seasonal variations may lead to dispersed data patterns and higher noise levels during non-epidemic seasons. Future research should incorporate vaccination data and explore additional data sources like behavioral patterns and environmental factors. External validation and detailed data preprocessing, such as smoothing or cross-validation, could enhance generalization.

This study demonstrates that multichannel data integration improves respiratory infectious disease

prediction accuracy and timeliness, with implications for public health responses. Ongoing research will refine these models for other health threats.

Conflicts of interest: No conflicts of interest.

Acknowledgments: The staff members at the Center for Disease Prevention and Control and Health Information Center for data verification.

Funding: Supported by the National Key Research and Development Program of China (grant no. 2022YFC2305103).

doi: 10.46234/ccdcw2025.234

* Corresponding authors: Qi Wang, wangqi_tj@hust.edu.cn; Sheng Wei, weis@sustech.edu.cn.

Copyright © 2025 by Chinese Center for Disease Control and Prevention. All content is distributed under a Creative Commons Attribution Non Commercial License 4.0 (CC BY-NC).

Submitted: September 19, 2025 Accepted: October 25, 2025 Issued: October 31, 2025

REFERENCES

- Iuliano AD, Roguski KM, Chang HH, Muscatello DJ, Palekar R, Tempia S, et al. Estimates of global seasonal influenza-associated respiratory mortality: a modelling study. Lancet 2018;391(10127):1285 – 300. https://doi.org/10.1016/S0140-6736(17)33293-2.
- Zhang YZ, Bambrick H, Mengersen K, Tong SL, Hu WB. Using internet-based query and climate data to predict climate-sensitive infectious disease risks: a systematic review of epidemiological evidence. Int J Biometeorol 2021;65(12):2203 – 14. https://doi.org/10.1007/ s00484-021-02155-4.
- Brownstein JS, Rader B, Astley CM, Tian HY. Advances in artificial intelligence for infectious-disease surveillance. N Engl J Med 2023;388 (17):1597 – 607. https://doi.org/10.1056/NEJMra2119215.

- Kraemer MUG, Tsui JLH, Chang SY, Lytras S, Khurana MP, Vanderslott S, et al. Artificial intelligence for modelling infectious disease epidemics. Nature 2025;638(8051):623 – 35. https://doi.org/ 10.1038/s41586-024-08564-w.
- Dong YH, Wang LP, Burgner DP, Miller JE, Song Y, Ren X, et al. Infectious diseases in children and adolescents in China: analysis of national surveillance data from 2008 to 2017. BMJ 2020;369:m1043. https://doi.org/10.1136/bmj.m1043.
- Nottmeyer LN, Sera F. Influence of temperature, and of relative and absolute humidity on COVID-19 incidence in England - A multi-city time-series study. Environ Res 2021;196:110977. https://doi.org/10. 1016/j.envres.2021.110977.
- 7. Krymova E, Béjar B, Thanou D, Sun T, Manetti E, Lee G, et al. Trend estimation and short-term forecasting of COVID-19 cases and deaths worldwide. Proc Natl Acad Sci USA 2022;119(32):e2112656119. https://doi.org/10.1073/pnas.2112656119.
- Prasanth S, Singh U, Kumar A, Tikkiwal VA, Chong PHJ. Forecasting spread of COVID-19 using google trends: a hybrid GWO-deep learning approach. Chaos Solitons Fractals 2021;142:110336. https:// doi.org/10.1016/j.chaos.2020.110336.
- Holmdahl I, Buckee C. Wrong but useful what covid-19 epidemiologic models can and cannot tell US. N Engl J Med 2020;383 (4):303 5. https://doi.org/10.1056/NEJMp2016822.
- Chin V, Samia NI, Marchant R, Rosen O, Ioannidis JPA, Tanner MA, et al. A case study in model failure? COVID-19 daily deaths and ICU bed utilisation predictions in New York state. Eur J Epidemiol 2020;35 (8):733 – 42. https://doi.org/10.1007/s10654-020-00669-6.
- 11. Morgan OW, Abdelmalik P, Perez-Gutierrez E, Fall IS, Kato M, Hamblion E, et al. How better pandemic and epidemic intelligence will prepare the world for future threats. Nat Med 2022;28(8):1526 8. https://doi.org/10.1038/s41591-022-01900-5.
- Uyeki TM, Hui DS, Zambon M, Wentworth DE, Monto AS. Influenza. Lancet 2022;400(10353):693 – 706. https://doi.org/10. 1016/S0140-6736(22)00982-5.
- 13. Milinovich GJ, Williams GM, Clements AC, Hu WB. Internet-based surveillance systems for monitoring emerging infectious diseases. Lancet Infect Dis 2014;14(2):160 8. https://doi.org/10.1016/S1473-3099 (13)70244-5.
- 14. Xu L, Zhou C, Luo ST, Chan DK, McLaws ML, Liang WN. Modernising infectious disease surveillance and an early-warning system: the need for China's action. Lancet Reg Health West Pac 2022;23:100485. https://doi.org/10.1016/j.lanwpc.2022.100485.
- Zhang R, Lai KY, Liu WH, Liu YH, Ma XW, Webster C, et al. Associations between short-term exposure to ambient air pollution and influenza: an individual-level case-crossover study in Guangzhou, China. Environ Health Perspect 2023;131(12):127009. https://doi.org/ 10.1289/EHP12145.
- Guo F, Zhang P, Do V, Runge J, Zhang K, Han ZS, et al. Ozone as an environmental driver of influenza. Nat Commun 2024;15(1):3763. https://doi.org/10.1038/s41467-024-48199-z.

¹ Department of Epidemiology and Biostatistics, School of Public Health, Tongji Medical College, Huazhong University of Science and Technology, Wuhan City, Hubei Province, China; ² Health Information Center of Wuhan, Wuhan City, Hubei Province, China; ³ School of Public Health and Emergency Management, Southern University of Science and Technology, Shenzhen City, Guangdong Province, China.

SUPPLEMENTARY MATERIAL

Model Introduction

This study constructed a prediction model for daily incidence of reported influenza cases using four channels surveillance data sources: hospital surveillance (H), Baidu Search Index (B), meteorological surveillance (M), and air pollutant surveillance (P). Six machine learning (ML) models were applied, covering common single and ensemble learning methods. The single models included linear regression (LR) and K-nearest neighbors (KNN). The ensemble learning models comprised random forest (RF) and extreme gradient boosting (XGBoost). Deep learning models included gated recurrent unit (GRU) and long short-term memory (LSTM). Model inputs (x) were different data combinations from the four sources, with outputs (y) as daily reported case numbers. Data from January 2023 to January 2025, were used, with 80% for training and 20% for testing. The study aimed to identify the optimal model for predicting influenza reported cases by comparing the predictive performance of different models.

Linear regression (LR) is a supervised ML algorithm that learns from labeled datasets to map data points to an optimal linear function. LR performs well in capturing linear relationships in time series and can handle small-scale data effectively. For formulas, see Equation [1], where β represents the partial regression coefficients and represents the residuals.

$$y = \beta_0 + \beta_1 x_1 + \beta_2 x_2 + \cdot \cdot \cdot + \beta_n x_n +$$
 (1)

K-Nearest Neighbors (KNN) is a versatile ML algorithm used for both classification and regression tasks. For regression, it predicts a value based on the average of the values of its k-nearest neighbors. The choice of k is critical as it balances the bias-variance trade-off. KNN is non-parametric, making no assumptions about the underlying data distribution, and is straightforward to implement.

Random Forest (RF) is an ensemble of tree-structured classifiers. Each tree predicts based on an independent and identically distributed random vector. In regression, it outputs numbers, trained on datasets from random vector distributions. By integrating multiple decision trees, RF reduces overfitting risk, handles nonlinear data and complex feature relationships, and is somewhat robust to missing data. For formulas, see Equation [2]. $_{\text{new}}^{\text{RF}}$ denote the RF's prediction for a new sample, which is the aggregated output from all decision trees in the model. m represent the number of decision trees in the RF. The prediction from the j-th decision tree for the new sample is denoted as $_{\text{l}_{j}}^{\text{tree}}$

$$\frac{RF}{new} = \frac{1}{m} \sum_{i=1}^{m} tree \atop l_i \tag{2}$$

XGBoost is an optimized distributed gradient-boosting library that implements ML algorithms in the Gradient Boosting framework. It's designed for efficiency, flexibility, and portability. XGBoost excels in performance, especially in nonlinear time-series problems. It can handle heterogeneous features and their complex interactions. The formula is shown in Equation [3]. $_{i}^{(t)}$ represents the model's prediction for the *t*-th sample, reflecting the latest prediction after cumulative optimization up to iteration t. $\sum_{k=1}^{t-1} f_k(x_i)$ is the cumulative prediction from previous iterations up to t-1. $f_t(x_i)$ denotes the prediction from the newly added tree at the *t*-th iteration, which aims to correct the model's prediction errors and bring the results closer to the true targets.

$$_{i}^{(t)} = \sum_{k=1}^{t-1} f_k(x_i) + f_t(x_i)$$
(3)

LSTM networks were developed to capture long-term dependencies in time-series data. An LSTM unit comprises three gated units and two states. The three gates are the forget gate (f_t) , input gate (i_t) , and output gate (o_t) , which regulate the information flow from the previous timestep. The two states are the hidden state (h_t) and cell state (c_t) . The hidden state ht acts as the short-term memory, passing information to the next timestep and the output layer. The cell state ct serves as the long-term memory, updated by the forget and input gates. Here's the structure in detail:

- Forget Gate Layer: Determines what information to discard from the cell state using a sigmoid function.
- Input Gate Layer: Updates the cell state with new information through a sigmoid function and a tanh function.
- Output Gate Layer: Decides the next hidden state using a sigmoid function and a tanh function. For the mathematical representation, the LSTM equations are as follows:

$$f_t = \sigma \left(W_f[C_{t-1}, h_{t-1}, x_t] + b_f \right) \tag{4}$$

$$i_{t} = \sigma \left(W_{i} \left[C_{t-1}, h_{t-1}, x_{t} \right] + b_{i} \right) \tag{5}$$

$$o_{t} = \sigma \left(W_{o} \left[C_{t-1}, h_{t-1}, x_{t} \right] + b_{o} \right) \tag{6}$$

GRU is an LSTM variant. It combines the LSTM's forget and input gates into a single update gate and merges the cell state (c_p) with the hidden state (h_p) , resulting in a simpler structure compared to the standard LSTM. This design reduces the number of parameters, enabling faster training or requiring less data for effective generalization.

Dataset Splitting

As shown in Supplementary Figure S1, the total cases of daily incidence of reported influenza cases in the city from January 2023, to January 2025, had two full peaks in 2023–2025 and an upward trend at the end of 2024. For each model, the dataset was sequentially split into training and testing sets at an 8:2 ratio. This gave the training set enough data for model fitting and the testing set a starting trend for prediction.

Model Evaluation

Model assessment used regression metrics: R², MAPE, MAE, and RMSE. R² indicates the percentage of variation in the target variable explained by the features. R² ranges from 0 to 1, with higher values indicating a better fit. MAPE measures the average percentage difference between predicted and actual values, reflecting the average deviation of predictions from true values. MAE is the average of absolute errors, providing a clear measure of prediction accuracy. RMSE, the square root of mean squared error, is widely used as it penalizes larger errors more than MAE. For MAPE, MAE, and RMSE, values closer to 0 indicate better model performance. The calculation equations for these metrics are presented below:

$$R^{2} = 1 - \frac{\sum_{i=1}^{n} (y_{i} - \hat{y}_{i})^{2}}{\sum_{i=1}^{n} (y_{i} - \bar{y}_{i})^{2}}$$
(7)

$$MAPE = \frac{1}{n} \sum_{i=1}^{n} \left| \frac{y_i - \hat{y}_i}{y_i} \right| \times 100\%$$
 (8)

$$MAE = \frac{1}{n} \sum_{i=1}^{n} \left| \hat{y}_i - y_i \right| \tag{9}$$

$$RMSE = \sqrt{\frac{1}{n} \sum_{i=1}^{n} (y_i - \hat{y}_i)^2}$$
 (10)

China CDC Weekly

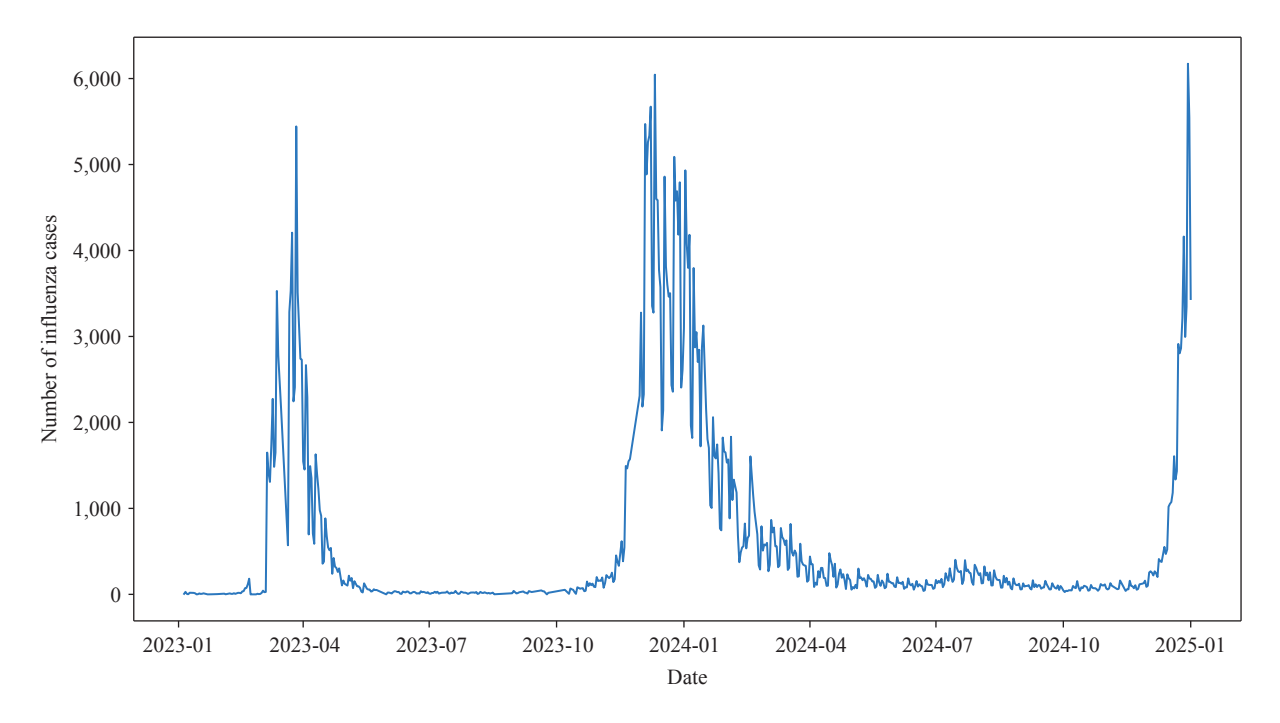
SUPPLEMENTARY TABLE S1. Different surveillance systems and dataset descriptions.

Multichannel surveillance data	Description	Timeline	Date range
Cases Report data			
Influenza_cases	Daily Reported Influenza Cases	1 day	Jan 5, 2023-Jan 1, 2025
Hospital Surveillance data			
visits	Fever Clinic Visits	1 day	Jan 5, 2023-Jan 1, 2025
Outpatients with respiratory symptoms	Daily Outpatients with respiratory symptoms		Jan 5, 2023-Jan 1, 2025
Fever	Outpatient chief complaint of fever	1 day	
Sore_throat	Outpatient chief complaint of sore throat	1 day	
Cough	Outpatient chief complaint of cough	1 day	
Runny_nose	Outpatient chief complaint of runny nose	1 day	
Myalgia	Outpatient chief complaint of myalgia	1 day	
Joint_pain	Outpatient chief complaint of joint pain	1 day	
Headache	Outpatient chief complaint of headache	1 day	
Dyspnea	Outpatient chief complaint of dyspnea	1 day	
Fatigue	Outpatient chief complaint of fatigue	1 day	
Multisymptoms	Outpatient chief complaint of two or more respiratory symptoms	1 day	
Search Engine Surveillance data	more respiratory symptoms		Jan 1, 2023-Jan 1, 2025
BSI1	Baidu search rank related with fever	1 day	
BSI2	Baidu search rank related with sore throat	1 day	
BSI3	Baidu search rank related with cough	1 day	
BSI4	Baidu search rank related with runny nose	1 day	
BSI5	Baidu search rank related with myalgia	1 day	
BSI6	Baidu search rank related with joint pain	1 day	
BSI7	Baidu search rank related with headache	1 day	
BSI8	Baidu search rank related with dyspnea	1 day	
BSI9	Baidu search rank related with fatigue	1 day	
Meteorological Surveillance data			Jan 1, 2023-Jan 1, 2025
Tmean	Daily average temperature	Every 3h per day	
Pmean	Daily average air pressure	Every 3h per day	
RHmean	Daily average relative humidity	Every 3h per day	
AHmean	Daily average absolute humidity	Every 3h per day	
WSmean	Daily average wind speed	Every 3h per day	
VISmean	Daily average visibility	Every 3h per day	
PRCPmean	Daily average precipitation	Every 3h per day	
Air pollutant Surveillance data			Jan 1, 2023-Jan 1, 2025
SO2	Daily average concentration of SO ₂	1 day	
NO2	Daily average concentration of NO ₂	1 day	
PM10	Daily average concentration of PM ₁₀	1 day	
PM2.5	Daily average concentration of PM _{2.5}	1 day	
CO	Daily average concentration of CO	1 day	
O3	Daily average concentration of O ₃	1 day	

SUPPLEMENTARY TABLE S2. Comparison of different window sizes of data between deep learning models.

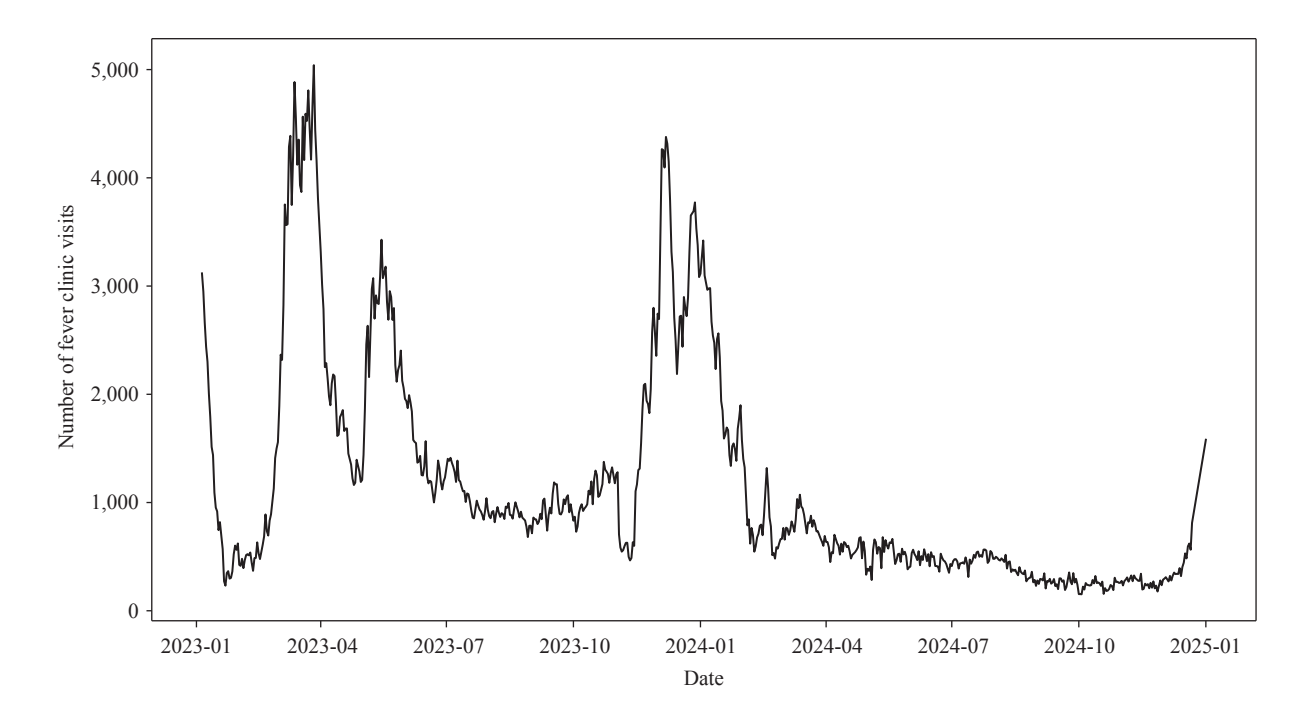
Madal wasfawaaaa	Window size					
Model performance	1 day	3 days	5 days	7 days	14 days	
MAE						
GRU	277.10	274.69	283.20	238.26	235.47	
LSTM	227.66	248.37	240.24	230.47	170.59	
MAPE (%)						
GRU	49.73	92.24	95.22	102.65	87.31	
LSTM	84.55	67.29	59.42	60.49	60.26	
RMSE						
GRU	767.65	688.28	707.67	561.88	581.57	
LSTM	651.43	653.26	638.03	607.43	453.23	
R^2						
GRU	0.40	0.52	0.50	0.68	0.68	
LSTM	0.57	0.67	0.59	0.64	0.81	

Abbreviation: MAE=mean absolute error; GRU=Gated Recurrent Unit; LSTM=Long Short-Term Memory; MAPE=mean absolute percentage error; RMSE=root mean square error; R²=coefficient of determination.

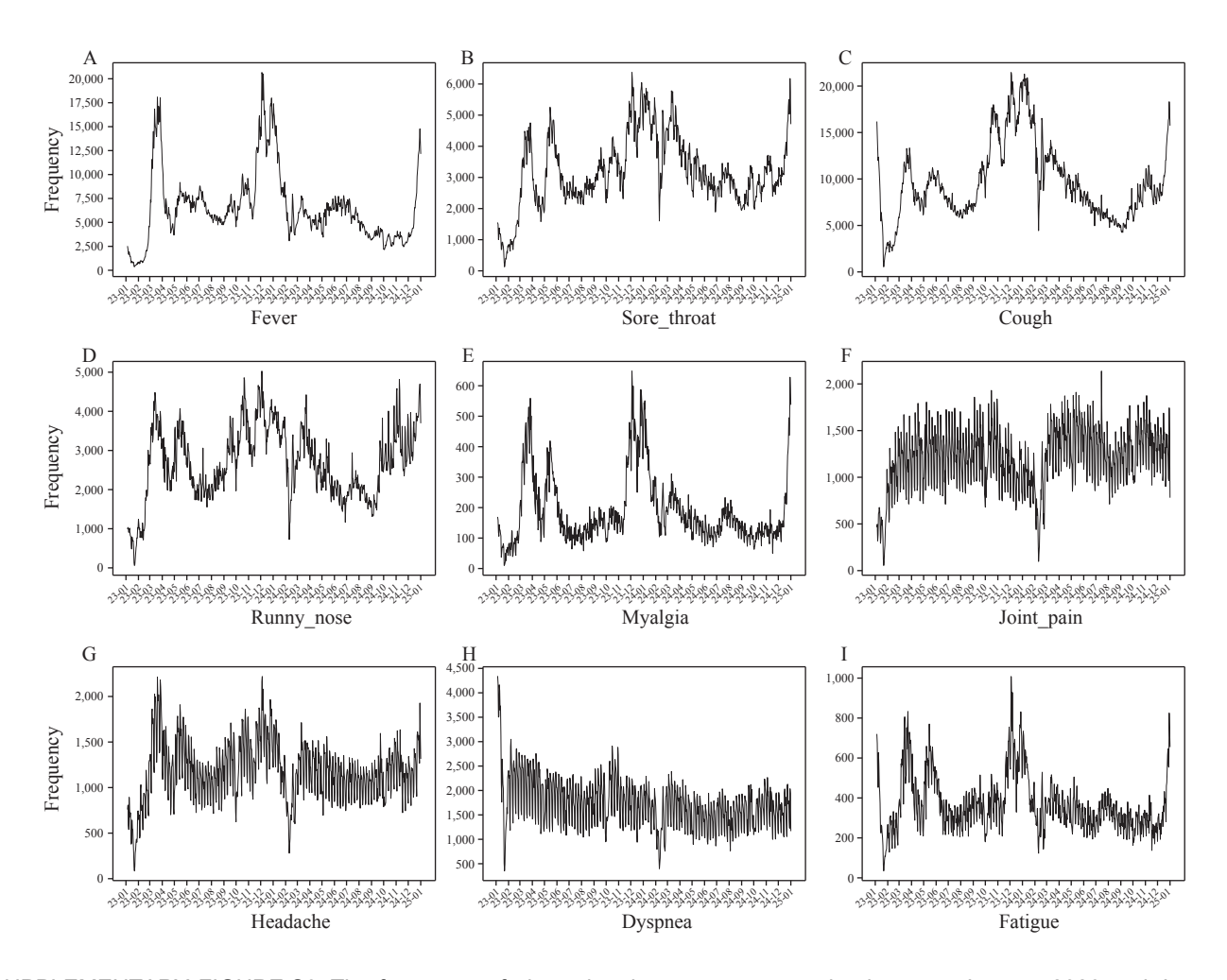


SUPPLEMENTARY FIGURE S1. The Reported Cases of Influenza every day between January 2023 and January 2025.

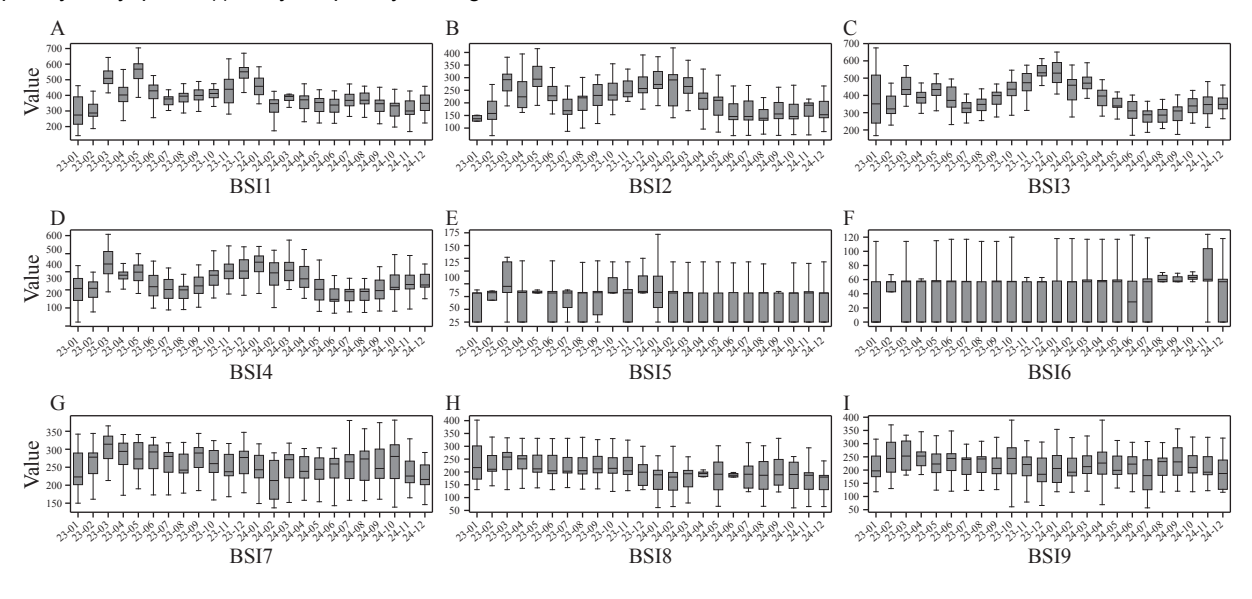
China CDC Weekly



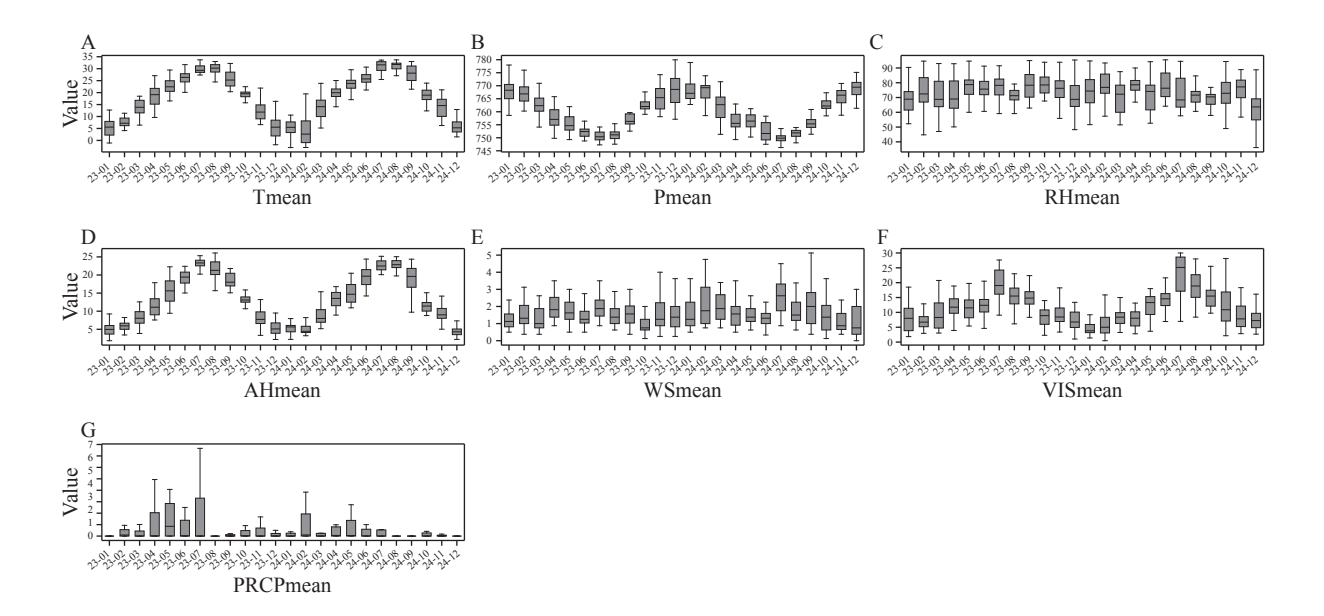
SUPPLEMENTARY FIGURE S2. The Fever Clinic Visits every day between January 2023 and January 2025.



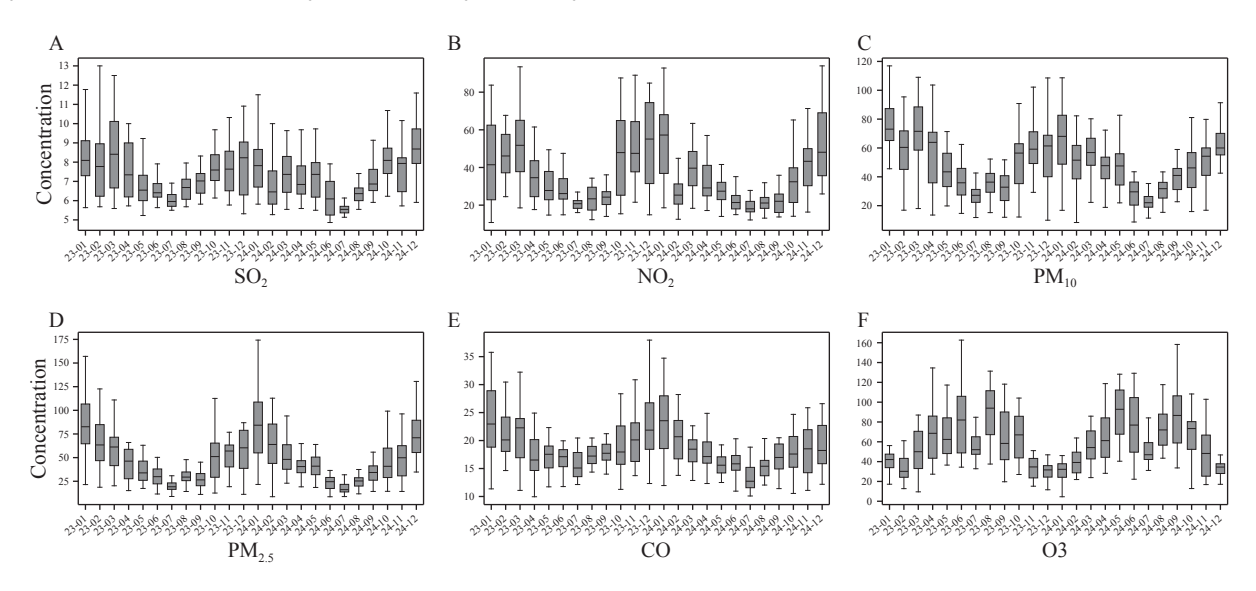
SUPPLEMENTARY FIGURE S3. The frequency of nine related symptoms every day between January 2023 and January 2025. (A) Daily frequency of fever; (B) Daily frequency of sore throat; (C) Daily frequency of cough; (D) Daily frequency of runny nose; (E) Daily frequency of myalgia; (F) Daily frequency of joint pain; (G) Daily frequency of headache; (H) Daily frequency of dyspnea; (I) Daily frequency of fatigue.



SUPPLEMENTARY FIGURE S4. The counts of nine related BSIs between January 2023 and January 2025. (A) Daily counts of BSI1; (B) Daily counts of BSI2; (C) Daily counts of BSI3; (D) Daily counts of BSI4; (E) Daily counts of BSI5; (F) Daily counts of BSI6; (G) Daily counts of BSI7; (H) Daily counts of BSI8; (I) Daily counts of BSI9.



SUPPLEMENTARY FIGURE S5. The description of daily climate factors between January 2023 and January 2025. (A) Daily mean temperature; (B) Daily mean air pressure; (C) Daily mean relative humidity; (D) Daily mean absolute humidity; (E) Daily mean wind speed; (F) Daily mean visibility; (G) Daily mean precipitation.



SUPPLEMENTARY FIGURE S6. The description of daily air pollutants between January 2023 and January 2025. (A) Daily concentration of SO2; (B) Daily concentration of NO2; (C) Daily concentration of PM10; (D) Daily concentration of PM2.5; (E) Daily concentration of CO; (F) Daily concentration of O3.

Outbreak Reports

Epidemiological and Genetic Characterization of Three H9N2 Viruses Causing Human Infections — Changsha City, Hunan Province, China, April 2025

Chaoyang Huang^{1,2,&}; Yi Liu^{1,&}; Zheng Huang³; Shuilian Chen³; Zhifei Zhan^{1,2}; Qianlai Sun¹; Ruchun Liu³; Liang Cai^{1,2,#}; Kaiwei Luo^{1,#}

Summary

What is already known about this topic?

A total of 117 H9N2 cases of human infection of Chinese origin had been reported to the World Health Organization (WHO) by May 9, 2025, with 22 of them originating in Hunan Province.

What is added by this report?

This article reported on the investigation of three new H9N2 avian influenza virus (AIV) infections detected in Changsha, Hunan Province, in April 2025. No epidemiological link was found among them. Exposure to live poultry was identified as the primary risk factor for infection. Sequence analysis of the three H9N2 AIVs showed a similarity of 99.71%–99.82% between hemagglutinin (HA), and the homology of the neuraminidase (NA) genes was 98.41%–99.83%. Although the tests showed that the HA had enhanced binding ability to upper respiratory tract cells' receptors, no evidence of sustained human-to-human transmission has been found so far.

What are the implications for public health practice?

This study indicated that H9N2 AIV remains a public health issue in China. We need to strengthen publicity and education efforts to inform people of the potential risk of avian influenza virus, especially to keep children away from poultry and poultry-related facilities, to effectively prevent the occurrence of avian influenza A(H9N2) infection.

ABSTRACT

Introduction: In April 2025, three suspected human cases of avian influenza were identified in Changsha, China. Laboratory testing confirmed three cases of H9N2 AIV infection. This report summarizes the epidemiological findings from cases and contact investigations, along with genetic characterization of

the isolated H9N2 strains.

Methods: Comprehensive epidemiological assessments were conducted for each confirmed case. Virus isolation and culture were performed using throat swab specimens obtained from the cases. Isolated H9N2 strains were sequenced using next-generation sequencing (NGS). HA and NA gene sequences were analyzed for homology; evolutionary trees were constructed; and key antigenic sites were examined to identify genetic features.

Results: All three cases were sporadic. No influenzalike illness was observed among close contacts or live poultry store employees during the 10-day medical monitoring period. Phylogenetic analysis indicated that the HA gene of all three H9N2 strains belonged to the A/Duck/Hong Kong/Y280/97 (Y280-like) within the Eurasian lineage. HA gene sequence homology was 99.7%-99.8%, and NA gene homology was 98.4%-99.8%. The HA protein cleavage site was identified as PSRSSR

GLF. Several HA protein site mutations were detected — H191N, A198T/V, Q226L, and Q234L — that had been previously associated with increased binding to receptors. HA-232H, 234L, and 236G support a binding preference for the human-type sialic acid- α -2,6-galactose receptors.

Conclusion: All three H9N2 avian influenza cases were mild and involved reported exposure to poultry or related environments. Genetic analysis revealed high homology of HA and NA among the isolated viruses. No epidemiological links were identified between cases, and no evidence was found of sustained human-to-human transmission. Continued avian influenza surveillance and public health education are warranted.

The H9N2 avian influenza virus (AIV) is the most prevalent avian influenza virus circulating among

poultry in China (1). While it primarily leads to economic losses in the poultry industry, it has also repeatedly crossed the species barrier to infect humans, raising public health concerns. Since 2015, China has consistently reported human H9N2 infections to the WHO, with 117 cumulative cases by May 9, 2025 (2). Among these, 19 cases were reported in Hunan Province by the end of 2024 (3), followed by three additional cases in April 2025. Therefore, it is crucial to closely monitor variations in H9N2 infectivity particularly its potential for cross-species transmission to humans. This study presents the epidemiological profiles of three human H9N2 cases detected through influenza-like illness (ILI) surveillance from Changsha, China, along with the molecular characteristics of the corresponding H9N2 viruses.

INVESTIGATION AND RESULTS

Human Infections with H9N2 AIVs

In April 2025, three new human H9N2 cases were reported in Changsha City, Hunan Province. All three cases were children and were confirmed as cases of H9N2 infection by Hunan Provincial CDC and Changsha CDC.

Case 1 was a seven-year-old female primary school student (patient 1), residing in Kaifu District. She developed a fever and cough on April 1 and sought care at the Pediatrics Department of Changsha First Hospital. She presented with a paroxysmal productive cough and was prescribed medication, remaining homebound from April 1 to 5 without exposure risks. On April 6, she returned for a follow-up.

Case 2 was a 16-month-old girl from Wangcheng District, who developed cough and low-grade fever (38.5 °C) on April 3. She was admitted to Changsha First Hospital on April 4 at 11:00 a.m. with a diagnosis of bronchopneumonia and was discharged on April 8 after recovery.

Case 3 was a five-year-old boy living in Kaifu District. He experienced fever onset on April 19 and sought medical care on April 20. Initial testing was positive for influenza A (H9N2), and his symptoms were resolved by April 25 (Table 1).

Epidemiological Investigation

Epidemiological investigations showed that none of the three cases had had pre-onset contact history with people experiencing fever or respiratory symptoms, and the three children had had no contact with each other. However, cases 1 and 2 had been exposed to live poultry markets, and case 3 had had contact with diseased and dead poultry.

Opposite the entrance of the community where Case 1 lives were six live poultry stores in Maojiaqiao Market, which was only 40 meters away. Case 1 passes by these live poultry stores every day on her way to school. On April 8, four environmental smear samples collected from her home tested negative for influenza A virus nucleic acid. Meanwhile, 13 environmental samples (7 smear samples and 6 water samples) from the live poultry stores all tested positive for influenza A virus. All three close contacts of Case 1 tested negative for influenza virus nucleic acid.

Case 2 had visited a live poultry store near her home within seven days before symptom onset. On April 16, four environmental samples collected from this store tested positive for H9N2 nucleic acid. All seven close contacts of Case 2 tested negative.

Case 3 bought a duckling as a pet on April 8, and the duckling died on April 15. Nucleic acid testing of four close contacts sampled on April 21 was negative for influenza virus nucleic acid.

H9N2 AIVs RNA Extraction and Sequencing

The H9N2 viruses were sequenced by Hunan Provincial CDC and Changsha CDC, with the following strain designations: Case 1: A/Hunan-Kaifu/1294/2025(H9N2), Case 2: A/Hunan-Kaifu/8210/2025(H9N2), and Case 3: A/Hunan-Kaifu/CS992/2025(H9N2). H9N2 AIVs RNA were extracted from the three patients using the Viral RNA Mini Kit (Qiagen, Germany). Reverse transcription

TABLE 1. Demography and epidemiology investigation of three H9N2 AIV cases in Changsha, April 2025.

Case	Sex	Age	District	Date of	Date of	Date of laboratory	Case	LPM	Contacted sick or dead
No.	Sex	(Years)	DISTRICT	onset	hospitalization	confirmation	type	contact	poultry
1	Female	7	Kaifu	2025.04.01	2025.04.01	2025.04.04	Outpatient	Yes	No
2	Female	1	Wangchen	g2025.04.03	2025.04.04	2025.04.11	Inpatient	Yes	No
3	Male	5	Kaifu	2025.04.19	2025.04.20	2025.04.24	Outpatient	Yes	Yes

Abbreviation: LPM=live poultry market; AIV=avian influenza virus.

and amplification were performed with the SuperScript® III One-Step RT-PCR System with Platinum Taq High Fidelity (Invitrogen, Carlsbad, USA). Libraries were constructed using the Nextera® XT Library Prep Kit (Illumina, USA). Sequencing was conducted on the MiSeq platform with the MiSeq V2 Kit (Illumina, USA). All library prep reagents, sequencing kits, and the sequencer were supplied by Illumina (USA). Raw FastQ data were assembled using CLC Genomics Workbench (Qiagen, Germany). The sequencing depth and coverage of HA and NA nucleic acids in H9N2 AIVs are presented in Supplementary Table S1 (available at https://weekly.chinacdc.cn/).

Bioinformatics Analysis

Global Initiative on Sharing All Influenza Data (GISAID) EpiFlu Database was used for sequence alignment of H9N2 hemagglutinin (HA) and neuraminidase (NA) genes. Reference sequences were downloaded for comparison. MAFFT (version 7.526, Advanced Industrial Science and Technology, Tokyo, Japan) performed multiple sequence alignment (4). Maximum-likelihood phylogenetic trees were constructed with 1,000 bootstrap replicates for statistical validation.

A/Hunan-Kaifu//8210/2025 A/Hunan-Kaifu/CS992/2025 Α A/Hunan-Kaifu/1294/2025 A/Hunan-Louxing/11086/2022 A/Anhui-Tianjiaan/11086/2022 Y280/G9 CVV A/Hunan/00468/2021|EPI ISL 3247004 A/Hong Kong/308/2014 Y280/G9 CVV A/Hunan-Chenzhou/45789/2015/EPI ISL 18044297 A/Hunan/44557/2015/EPI ISL 234468 A/Hunan/44558/2015/EPI ISL 203644 Anhui-Lujiang/39/2018|EPI ISL 330737 Y280/G9 CVV A/Hunan/11173/2020/FPLISL 548682 Y280 A/Hunan/34179/2018|EPI ISL 345236 /Hunan/37286/2017|EPI ISL 337281 A/Hunan/42088/2017/EPI ISL 337279 A/chicken/Shandong/3424/2016|EPI ISL 505068 A/Chicken/Jiangsu/WJ57/2012|EPI ISL 944031 A/Hunan-Lengshuitan/11197/2013/EPLISL 18044287 A/Duck/Hong Kong/Y280/97|EPI ISL 1266 A/chicken/Hong Kong/G9/1997|EPI ISL 146698 Y280/G9 A/Chicken/Guangdong/SS/94|EPI ISL 68726 A/Chicken/Shandong/6/96|EPI ISL 2240 A/Chicken/Shanghai/F/98|EPI ISL 68579 A/Chicken/Beijing/1/94/EPI ISL 1270 A/quail/Hong Kong/G1/1997|EPI ISL 3144464] G1 A/duck/Hong Kong/Y439/1997/EPI ISL 146723 - A/turkev/Wisconsin/1/1966|EPI ISL 8917 0.02

Phylogenetic analysis revealed that the HA and NA genes of all three viruses clustered within the A/Duck/Hong Kong/Y280/97(H9N2) (Y280-like) evolutionary lineage of the Eurasian branch (Figure 1). Nucleotide similarities among the three strains were 99.71%–99.82% for HA and 98.41%–99.83% for NA. Compared with the reference strain A/Hunan-Louxing/11086/2022(H9N2) (LX11086) isolated in Loudi, Hunan Province, in 2022, HA gene homology was 96.8%–96.9%, and NA gene homology was 95.0%–95.2%.

The basic local alignment search tool (BLAST) in the GISAID EpiFlu database indicated that the HA genes of the three H9N2 AIVs shared high homology (98.41%–98.51%) with A/chicken/Vietnam/NCVD-23CB2V7S5-38/2023(H9N2), a strain isolated from Vietnamese chickens. The NA genes were highly homologous (97.42%–97.57%) to A/environment/Xiamen/01/2021(H9N2) (Table 2).

Protein sequence analysis using LX11086 as a reference revealed that the HA cleavage site sequences of HA1 and HA2 of all viruses were PSRSSR↓GLF (positions 333aa–341aa), which did not have a continuous acidic amino acid (lysine, arginine, or histidine) sequence, consistent with low-pathogenicity

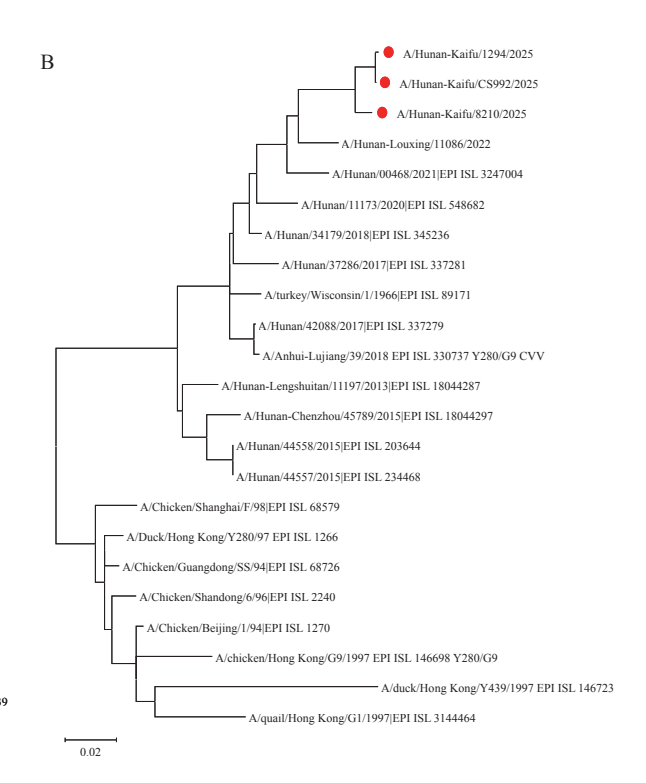


FIGURE 1. Maximum likelihood phylogenetic relationships of H9N2 viruses. (A) HA genes; (B) NA genes. Note: Red circle means The H9N2 AIVs researched in this study. Abbreviation: HA=hemagglutinin; NA=neuraminidase; AIV=avian influenza virus.

TABLE 2. Similarity of HA and NA segments of three H9N2 AIVs analyzed by online BLAST.

Case NO.	Virus	Date of collection	Abbreviation	Segment	Strain with the highest similarity in GISAID	GISAID ID	Similarity (%)
1	A/Hunan-Kaifu/	2025.04.02	2 KF1294	HA	A/chicken/Vietnam/NCVD-23CB2V7S5-38/2023	EPI4316643	98.51
'	1294/2025(H9N2)			NA	A/environment/Xiamen/01/2021	EPI2161506	97.42
2	A/Hunan-Kaifu/	2025.04.07	7 KF8210	HA	A/chicken/Vietnam/NCVD-23CB2V7S5-38/2023	EPI4316643	98.46
2	² 8210/2025(H9N2)	2025.04.07		NA	A/environment/Xiamen/01/2021	EPI2161506	97.57
3	A/Hunan-Kaifu/	n-Kaifu/ 2025.04.21	5.04.21 CS992	HA	A/chicken/Vietnam/NCVD-23CB2V7S5-38/2023	EPI4316643	98.51
3 CS992/2025(H9N2)	2) 2023.04.21	03992	NA	A/environment/Xiamen/01/2021	EPI2161506	97.56	

Abbreviation: BLAST=basic local alignment search tool; GISAID=Global Initiative on Sharing All Influenza Data; HA=hemagglutinin; NA=neuraminidase: AIV=avian influenza virus.

avian influenza virus (LPAIV) H9 strains. Analysis of receptor-binding sites showed that the HA proteins had mutations at amino acid positions H191N, A198V, Q226L, and Q234L, which potentially enhanced the binding ability of the virus to the receptor (5–6). The amino acids of the HA protein were N232H, Q234L, and 235M, binding to the human receptor sialic acid- α 2,6-galactose, and G236 is a typical feature of avian viruses. No resistance-associated mutations were detected in the NA protein (Table 3).

PUBLIC HEALTH RESPONSE

The Kaifu CDC and Wangcheng CDC have conducted a 10-day medical observation on the close contacts of the three cases and the employees of the related live poultry stores. None of them developed influenza-like symptoms such as fever and cough. The disease control departments have also strengthened the monitoring of avian influenza in live poultry markets and assisted hospitals with training for the prevention and control of avian influenza in ILI cases.

The Changsha CDC conducted emergency monitoring of the sources of chickens and ducks in the live poultry stores of Case 1 and Case 2, as well as the Shuiduhe Market and Huangxing Town Market, on April 27, 2025. A total of 62 environmental samples were collected, and the nucleic acid test results showed that 33 samples were positive for H9N2 AIV, and 2 samples were positive for H5 AIV.

DISCUSSION

Avian influenza viruses are categorized into highly pathogenic avian influenza virus (HPAIV) and LPAIV based on their pathogenicity. HPAIV consists of subtypes H5 (e.g., H5N1, H5N6) and H7 (e.g., H7N9), while H9N2 is the predominant LPAIV.

Most human infections with H9N2 result in mild and self-limiting symptoms, so the public and clinicians paid less attention compared to H5 or H7 infections. However, H9N2 AIV demonstrates a notable capacity for cross-species transmission. Serological evidence indicated a higher seropositivity rate among poultry workers for H9N2 than for H5N1 or H7N9 (7). Moreover, genetic analyses reveal that H9N2 frequently contributes internal gene segments to emerging reassortant viruses, such as H3N8, H10N8, H5N6, and H7N9. Co-circulation of LPAIVs with other subtypes provided opportunities for the novel AIVs to cross the species barrier.

Three children infected with H9N2 AIV were identified in Changsha in April 2025, and no epidemiological links were found between these mild and sporadic cases. Genetic analysis showed that the H9N2 viruses had enhanced binding ability to upper respiratory tract receptors, particularly the α 2,6-sialic acid receptors.

During the infection cycle of the influenza virus, the binding of the HA protein to the sialic acid receptor on the cell surface is a prerequisite for AIV to infect the host. The surface receptor of human upper respiratory tract epidermal cells is the α 2,6-sialic acid receptor, which is species-specific to the α 2,3-sialic acid receptor of avian cells. The mutations of Q234L in the AIV HA protein enabled an AIV-prioritized binding receptor shift from α 2,3-sialic acid to α 2,6-sialic acid. Liu et al. found that between 2005 and 2011, the H9N2 subtype of AIV acquired a stronger binding ability to the α 2,6-sialic acid receptor (8).

As the main antigenic proteins of the influenza virus, the HA protein and NA protein are subject to recognition by the host immune system and induced immune responses, thus facing greater immune selection pressure. Variations in the HA sequence may have a significant impact on the virulence (high pathogenicity and low pathogenicity), transmissibility,

TABLE 3. Molecular features of the genes of H9N2 viruses isolated from humans.

Virus	LX11086	KF1294	KF8210	CS992	
Cleavage peptides 333–341		PSRSSRGLF	PSRSSRGLF	PSRSSRGLF	PSRSSRGLF
	109	Υ	Υ	Υ	Υ
	161	W	W	W	W
	163	N	N	N	N
	191	N	N	N	N
Receptor binding sites of HA	198	V	V	V	V
	202	L	L	L	L
	203	Υ	Υ	Υ	Υ
	226	L	L	L	L
	232–236	NGLMG	HGLMG	HGLMG	HGLMG
	281	L	L	L	L
Antinonio sitos of LIA	285	S	S	S	S
Antigenic sites of HA	296	G	G	G	G
	334	S	S	S	S
	62–64	del	del	del	del
Sites of NA	119	E	E	E	E
	292	R	R	R	R

Abbreviation: HA=hemagglutinin; NA=neuraminidase.

and host specificity (infection of humans, poultry, or other animals) of the virus. Mutations at the key receptor binding sites of the HA protein can change the ability of the virus to infect different tissues and organs. If AIV HA acquires a stronger ability to bind to the receptors of lower respiratory tract cells, AIV will be more likely to invade the lungs, and its pathogenicity and infection consequences will be significantly enhanced. The key sites of the NA sequence are related to the sensitivity of the virus to influenza virus drugs. Mutations such as E119D/I/V and R292K, which increased the drug resistance of the influenza virus, have not been found in the three strains of the H9N2 virus, indicating that clinical drugs (Oseltamivir, Zanamivir) are still effective in the treatment of the H9N2 influenza virus. All NA proteins of the three virus strains had three amino acid residues TEI (positions 62-64) deletion in the NA stems, which was consistent with the AIV sequence of the Y280 lineage (9). The NA proteins were more efficient at hydrolyzing sialic acid, promoting viral replication and transmission, and therefore better suited to transmission from wild birds to poultry (10).

The H9N2 avian influenza outbreaks pose significant challenges to public health systems. It is imperative to strengthen environmental surveillance in live poultry markets, improve early recognition of AIVs

in clinical settings — particularly in cases of unexplained pneumonia — and enhance interdisciplinary collaboration among agricultural, public health, and market regulatory agencies. Popularizing knowledge about AIV is equally imperative. The public should minimize contact with chicken, ducks, and other birds in areas known to be affected by AIVs, including markets and stores where live poultry may be sold or slaughtered (11).

Conflicts of interest: No conflicts of interest.

Acknowledgments: Staff members at Kaifu CDC and Wangcheng CDC.

Funding: Supported by grants from Hunan Provincial Health Commission Major Scientific Research Program for High-Level Health Talents (R2023067), Central Guidance on Local Science and Technology Development Fund of Hunan Province (2024ZYC031-5), Scientific Research Project of Hunan Provincial Health Commission (A202312066016, D202312069067), and Hunan Provincial Center for Disease Control and Prevention Qinghe Foundation (QHJJ2024001).

doi: 10.46234/ccdcw2025.235

^{*} Corresponding authors: Kaiwei Luo, cfk@hncdc.com; Liang Cai, cailiang@hncdc.com.

¹ Hunan Provincial Center for Disease Control and Prevention, Hunan Provincial Academy of Preventive Medicine, Changsha City, Hunan

China CDC Weekly

Province, China; ² Hunan Provincial Key Laboratory of Microbial Molecular Biology, Changsha City, Hunan Province, China; ³ Changsha Center for Disease Control and Prevention, Changsha City, Hunan Province, China.

& Joint first authors.

Copyright © 2025 by Chinese Center for Disease Control and Prevention. All content is distributed under a Creative Commons Attribution Non Commercial License 4.0 (CC BY-NC).

Submitted: July 30, 2025 Accepted: October 21, 2025 Issued: October 31, 2025

REFERENCES

- Bi YH, Li J, Li SQ, Fu GH, Jin T, Zhang C, et al. Dominant subtype switch in avian influenza viruses during 2016-2019 in China. Nat Commun 2020;11(1):5909. https://doi.org/10.1038/s41467-020-19671-3
- World Health Organization. Avian influenza weekly update number 996. 2025. https://cdn.who.int/media/docs/default-source/wpro---documents/emergency/surveillance/avian-influenza/ai_20250509. pdf?sfvrsn=d06dd936_1&download=true. [2025-5-18].
- Zhao SL, Huang CY, Liu ZY, Sun QL, Zeng G, Wang XL, et al. Surveillance for avian influenza A (H9N2) virus in human infection cases and H9 subtype avian influenza virus in the external environment in Hunan, 2013-2022. Dis Surveill 2024;39(7):836 – 40. https://doi. org/10.3784/jbjc.202305160219.

- Nakamura T, Yamada KD, Tomii K, Katoh K. Parallelization of MAFFT for large-scale multiple sequence alignments. Bioinformatics 2018;34(14):2490 – 2. https://doi.org/10.1093/bioinformatics/bty121.
- Suttie A, Deng YM, Greenhill AR, Dussart P, Horwood PF, Karlsson EA. Inventory of molecular markers affecting biological characteristics of avian influenza A viruses. Virus Genes 2019;55(6):739 – 68. https:// doi.org/10.1007/s11262-019-01700-z.
- Wan HQ, Perez DR. Quail carry sialic acid receptors compatible with binding of avian and human influenza viruses. Virology 2006;346(2): 278 – 86. https://doi.org/10.1016/j.virol.2005.10.035.
- Yu Q, Liu LQ, Pu J, Zhao JY, Sun YP, Shen GN, et al. Risk perceptions for avian influenza virus infection among poultry workers, China. Emerg Infect Dis 2013;19(2):313 – 6. https://doi.org/10.3201/ eid1902.120251.
- 8. Liu QZ, Zhao LC, Guo YN, Zhao YZ, Li YF, Chen N, et al. Antigenic evolution characteristics and immunological evaluation of H9N2 avian influenza viruses from 1994-2019 in China. Viruses 2022;14(4):726. https://doi.org/10.3390/v14040726.
- Arai Y, Elgendy EM, Daidoji T, Ibrahim MS, Ono T, Sriwilaijaroen N, et al. H9N2 influenza virus infections in human cells require a balance between neuraminidase sialidase activity and hemagglutinin receptor affinity. J Virol 2020;94(18):e01210 – 20. https://doi.org/10.1128/JVI. 01210-20.
- Broecker F, Zheng A, Suntronwong N, Sun WN, Bailey MJ, Krammer F, et al. Extending the stalk enhances immunogenicity of the influenza virus neuraminidase. J Virol 2019;93(18):e00840 – 19. https://doi.org/ 10.1128/JVI.00840-19.
- 11. World Health Organization. Public health resource pack for countries experiencing outbreaks of influenza in animals. 2023. https://iris.who.int/server/api/core/bitstreams/c4c57a50-2f61-46a5-a6b7-d081a319 ddd5/content. [2025-9-9].

SUPPLEMENTARY MATERIAL

SUPPLEMENTARY TABLE S1. Sequencing depth and coverage of HA and NA of three H9N2 AIVs.

Virus	Segment	Sequencing depth	Sequencing coverage (%)
VE1204	HA	47,422	100.00
KF1294	NA	33,462	100.00
KF8210	HA	4,118	100.00
	NA	274	100.00
CS992	HA	31,243	100.00
	NA	15,614	100.00

Abbreviation: HA=hemagglutinin; NA=neuraminidase; AIV=avian influenza virus.

Youth Editorial Board

Director Lei Zhou

Vice Directors Jue Liu Tiantian Li Tianmu Chen

Members of Youth Editorial Board

Jingwen Ai Li Bai Yuhai Bi Yunlong Cao Gong Cheng Liangliang Cui Meng Gao Jie Gong Yuehua Hu Xiang Huo Jia Huang Xiaolin Jiang Yu Ju Min Kang Huihui Kong Lingcai Kong Shengjie Lai Fangfang Li Jingxin Li **Huigang Liang** Di Liu Jun Liu Li Liu Yang Liu Chao Ma Yang Pan Zhixing Peng Menbao Qian Tian Qin Shuhui Song Kun Su Song Tang Bin Wang Jingyuan Wang Linghang Wang Qihui Wang Feixue Wei Xiaoli Wang Xin Wang Yongyue Wei Zhiqiang Wu Meng Xiao Tian Xiao Wuxiang Xie Lei Xu Lin Yang Canging Yu Lin Zeng Yi Zhang Yang Zhao Hong Zhou

Indexed by Science Citation Index Expanded (SCIE), Social Sciences Citation Index (SSCI), PubMed Central (PMC), Scopus, Chinese Scientific and Technical Papers and Citations, and Chinese Science Citation Database (CSCD)

Copyright © 2025 by Chinese Center for Disease Control and Prevention

Under the terms of the Creative Commons Attribution-Non Commercial License 4.0 (CC BY-NC), it is permissible to download, share, remix, transform, and build upon the work provided it is properly cited. The work cannot be used commercially without permission from the journal. References to non-China-CDC sites on the Internet are provided as a service to CCDC Weekly readers and do not constitute or imply endorsement of these organizations or their programs by China CDC or National Health Commission of the People's Republic of China. China CDC is not responsible for the content of non-China-CDC sites.

The inauguration of *China CDC Weekly* is in part supported by Project for Enhancing International Impact of China STM Journals Category D (PIIJ2-D-04-(2018)) of China Association for Science and Technology (CAST).



Vol. 7 No. 44 Oct. 31, 2025

Responsible Authority

National Disease Control and Prevention Administration

Sponsor

Chinese Center for Disease Control and Prevention

Editing and Publishing

China CDC Weekly Editorial Office No.155 Changbai Road, Changping District, Beijing, China Tel: 86-10-63150501, 63150701 Email: weekly@chinacdc.cn

CSSN

ISSN 2096-7071 (Print) ISSN 2096-3101 (Online) CN 10-1629/R1